


5-2012

CHEMOSENSITIZATION OF HEPATOCELLULAR CARCINOMA TO GEMCITABINE BY NON-INVASIVE RADIOFREQUENCY FIELD-INDUCED HYPEROTHERMIA

Mustafa Raof

Follow this and additional works at: http://digitalcommons.library.tmc.edu/utgsbs_dissertations

 Part of the [Genetic Processes Commons](#), [Hepatology Commons](#), [Laboratory and Basic Science Research Commons](#), [Medical Pharmacology Commons](#), [Molecular Biology Commons](#), [Neoplasms Commons](#), [Nucleic Acids, Nucleotides, and Nucleosides Commons](#), [Pharmacology Commons](#), and the [Surgery Commons](#)

Recommended Citation

Raof, Mustafa, "CHEMOSENSITIZATION OF HEPATOCELLULAR CARCINOMA TO GEMCITABINE BY NON-INVASIVE RADIOFREQUENCY FIELD-INDUCED HYPEROTHERMIA" (2012). *UT GSBS Dissertations and Theses (Open Access)*. Paper 244.

This Thesis (MS) is brought to you for free and open access by the Graduate School of Biomedical Sciences at DigitalCommons@The Texas Medical Center. It has been accepted for inclusion in UT GSBS Dissertations and Theses (Open Access) by an authorized administrator of DigitalCommons@The Texas Medical Center. For more information, please contact laurel.sanders@library.tmc.edu.

CHEMOSENSITIZATION OF HEPATOCELLULAR CARCINOMA TO GEMCITABINE
BY NON-INVASIVE RADIOFREQUENCY FIELD-INDUCED HYPERTHERMIA

by
Mustafa Raoof, MD

APPROVED: □□□□

Steven A. Curley, MD (Advisor)

Gary E. Gallick, PhD

□□□□

Anil Sood, MD

□□□□

Sunil Krishnan, MD

□□□□

Lon J. Wilson, PhD

APPROVED:

□ _____

Dean, The University of Texas
Graduate School of Biomedical Sciences at Houston

**CHEMOSENSITIZATION OF HEPATOCELLULAR CARCINOMA TO
GEMCITABINE BY NON-INVASIVE RADIOFREQUENCY FIELD-INDUCED
HYPERTHERMIA**

□□□A

THESIS

Presented to the Faculty
of □The University of Texas □
Health Science Center at Houston □
and □
The University of Texas
□M.D. Anderson Cancer Center □
Graduate School of Biomedical Sciences □
in Partial Fulfillment
of the Requirements

for the Degree of

MASTER OF SCIENCE

□□by

Mustafa Raof, MD

Houston, Texas

May 2012

Dedicated to my wife and parents

ACKNOWLEDGEMENTS

I thank my supervisor Dr Steven A. Curley, for his support of my research ideas, his unfaltering conviction in my capabilities, his appropriately timed guidance and personal support. I express sincere gratitude to the members of my committee, Dr Anil Sood, Dr Gary E. Gallick, Dr Sunil Krishnan and Dr Lon J. Wilson for their valuable time, commitment, suggestions and patience. I am also grateful to the members of Dr Curley's lab group, past and present for their willing help and useful recommendations.

**CHEMOSENSITIZATION OF HEPATOCELLULAR CARCINOMA TO
GEMCITABINE BY NON-INVASIVE RADIOFREQUENCY FIELD-INDUCED
HYPERTHERMIA**

Publication No. _____

Mustafa Raoof, MD

Supervisory Professor: Steven A. Curley, MD

Gemcitabine is a potent nucleoside analogue against solid tumors however drug resistance rapidly emerges. Removal of gemcitabine incorporated in the DNA by repair mechanisms could potentially contribute to resistance in chemo-refractory solid tumors. In this study, we evaluated homologous recombination repair of gemcitabine-stalled replication forks as a potential mechanism contributing to resistance. We also studied the effect of hyperthermia on homologous recombination pathway to explain the previously reported synergy between gemcitabine and hyperthermia. We found that hyperthermia degrades and inhibits localization of Mre11 to gemcitabine-stalled replication forks. Furthermore, gemcitabine-treated cells that were also treated with hyperthermia demonstrate a prolonged passage through late S/ G2 phase of cell cycle in comparison to cells treated with gemcitabine alone. This coincides with inhibition of resolution of γ H2AX foci. Our findings also demonstrate that thermal sensitization of human hepatocellular carcinoma cell lines to gemcitabine is mediated through an Mre11-dependent homologous recombination repair pathway. Combination of non-invasive radiofrequency field-induced hyperthermia and gemcitabine was superior to either therapy alone ($p < 0.05$) in two different orthotopic murine models of hepatocellular carcinoma. This study provides mechanistic understanding and support of homologous recombination inhibiting-strategies, such as non-invasive radiofrequency field-induced hyperthermia, to overcome resistance to gemcitabine in refractory human solid tumors.

TABLE OF CONTENTS

Approval Page.....	i
Title page.....	ii
Acknowledgements.....	iv
Abstract.....	v
List of illustrations.....	viii
List of Abbreviations.....	x
1. INTRODUCTION.....	1
1.1 HEPATOCELLULAR CARCINOMA – AN EMERGING HEALTH PROBLEM.....	1
1.2 CURRENT TREATMENT STRATEGIES.....	2
1.3 GEMCITABINE AND RESISTANCE MECHANISMS.....	4
1.4 REPAIR OF MAMMALIAN STALLED REPLICATION FORKS.....	9
1.5 THERMOLABILE TARGETS IN HOMOLOGOUS RECOMBINATION PATHWAY.....	11
1.6 HYPOTHESIS AND SPECIFIC AIMS.....	14
2. MATERIALS AND METHODS.....	16
2.1 CELL LINES, REAGENTS AND TRANSFECTION.....	16
2.2 PROTEIN ELECTROPHORESIS AND IMMUNOBLOTTING.....	19
2.3 IMMUNOCYTOCHEMISTRY.....	20
2.4 CLONOGENIC ASSAYS.....	22
2.5 CELL CYCLE ANALYSIS.....	22
2.6 MOUSE MODEL OF HEPATOCELLULAR CARCINOMA.....	23
2.7 RADIOFREQUENCY GENERATOR SETUP.....	26
2.8 THERMAL IMAGING AND FIBER OPTIC THERMOGRAPHY.....	27

2.8 IMMUNOHISTOCHEMISTRY	29
2.9 STATISTICAL ANALYSES	30
3. RESULTS	31
3.1 EFFECT OF MODERATE HYPERTHERMIA ON HRR-PATHWAY PROTEINS.....	31
3.2 LOCALIZATION OF HRR-PATHWAY PROTEINS TO GEMCITABINE-STALLED REPLICATION FORKS.....	34
3.3 CELL CYCLE ALTERATIONS	43
3.4 CLONOGENIC SURVIVAL & VIABILITY.....	48
3.5 ANIMAL MODEL STUDIES.....	52
3.6 HISTOLOGICAL ANALYSIS OF HUMAN HCC XENOGRAFTS FROM MICE	63
4. DISCUSSION	71
5. CONCLUSION AND FUTURE STUDIES	76
BIBLIOGRAPHY	78
VITA	93

LIST OF ILLUSTRATIONS

FIGURE 1.	RADIOFREQUENCY GENERATOR AND FIBER OPTIC PROBE PLACEMENT.....	28
FIGURE 2.	EFFECT OF MODERATE HYPERTHERMIA ON HRR-PATHWAY PROTEINS.....	32-33
FIGURE 3.	GEMCITABINE-STALLED REPLICATION FORKS ARE MARKED BY γ -H2AX FOCI.....	37
FIGURE 4.	HYPERTHERMIA-INDUCED γ -H2AX FOCI ARE S-PHASE SPECIFIC.....	38
FIGURE 5.	GEMCITABINE AND HYPERTHERMIA-STALLED REPLICATION FORKS RECRUIT RPA.....	39
FIGURE 6.	INHIBITION OF MRE11 RECRUITMENT AT GEMCITABINE-STALLED REPLICATION FORKS BY HYPERTHERMIA.....	40
FIGURE 7.	INHIBITION OF RAD51 RECRUITMENT AT GEMCITABINE-STALLED REPLICATION FORKS BY HYPERTHERMIA.....	41
FIGURE 8.	QUANTIFICATION OF DATA PRESENTED IN FIGURE 3-7.....	42
FIGURE 9.	HYPERTHERMIA INHIBITS POST-REPLICATION RECOMBINATION REPAIR AT GEMCITABINE STALLED REPLICATION FORKS.....	45-47
FIGURE 10.	HYPERTHERMIA SENSITIZES HEPATOCELLULAR CARCINOMA CELLS TO GEMCITABINE IN A DOSE-DEPENDENT MANNER.....	50
FIGURE 11.	HYPERTHERMIA-INDUCED GEMCITABINE SENSITIVITY OF HEPATOCELLULAR CARCINOMA CELLS IS VIA MRE11-DEPENDENT PATHWAY.....	51
FIGURE 12.	ANIMAL MODEL CHARACTERIZATION.....	52-53
FIGURE 13.	THERMAL DOSE QUANTIFICATION IN HEP3B XENOGRAFTS UNDER RF FIELD EXPOSURE (13.56 MHz, 600W).....	56
FIGURE 14.	EFFICACY OF GEMCITABINE AND RF COMBINATION THERAPY IN MICE BEARING HEP3B XENOGRAFTS.....	59
FIGURE 15.	EFFICACY OF GEMCITABINE AND RF COMBINATION THERAPY IN MICE BEARING HEPG2 XENOGRAFTS.....	60

FIGURE 16.	EFFICACY OF GEMCITABINE AND MIRIN COMBINATION THERAPY IN MICE BEARING HEP3B XENOGRAFTS.....	62
FIGURE 17.	IMMUNOHISTOCHEMICAL ANALYSIS FOR PROLIFERATION, APOPTOSIS AND AUTOPHAGY ...	66
FIGURE 18.	INHIBITION OF MRE11 LOCALIZATION TO STALLED FORKS <i>IN VIVO</i>	67
FIGURE 19.	INHIBITION OF RAD51 LOCALIZATION TO STALLED FORKS <i>IN VIVO</i>	68
FIGURE 20.	RF EXPOSURE INHIBITS RESOLUTION OF GEMCITABINE-INDUCED DNA DAMAGE IN HEP3B XENOGRAFTS.....	69- 70

LIST OF ABBREVIATIONS

ARA-C	ARABINOSIDE CYTOSINE
ATM	ATAXIA TELANGIECTASIA MUTATED
ATCC	AMERICAN TYPE CULTURE COLLECTION
BRDU	BROMODEOXYURIDINE
CEM43	CUMULATIVE EQUIVALENT MINUTES AT 43°C
CC-3	CLEAVED CASPASE-3
CHAPS	3-[(3-CHOLAMIDOPROPYL) DIMETHYLAMMONIO]-1- β -PROPANESULFONATE
DCK	DEOXYCYTIDINE KINASE
dFdCMP	DEOXYCYTIDINE MONO-PHOSPHATE
dFdCDP	DEOXYCYTIDINE DI-PHOSPHATE
dFdCTP	DEOXYCYTIDINE TRI-PHOSPHATE
DCDA	DEOXYCYTIDINE DEAMINASE (DCDA),
dNTP	DEOXY-NUCLEOTIDE TRI-PHOSPHATE
DAPI	4',6-DIAMIDINO-2-PHENYLINDOLE
HCC	HEPATOCELLULAR CARCINOMA
hNT	NUCLEOTIDE TRANSPORTER
hENT1	EQUILIBRATIVE TYPE NUCLEOTIDE TRANSPORTER 1 (hENT1)
HRR	HOMOLOGOUS RECOMBINATION REPAIR
HT	HYPERTHERMIA
I.P.	INTRA-PERITONEAL
MMR	MISMATCH REPAIR
MRN	MRE11-RAD50-NBS1
NTP	NUCLEOTIDE TRIPHOSPHATES

NA	NUMERICAL APERTURE
N/A	NOT APPLICABLE
PARP1	POLY (ADP-RIBOSE) POLYMERASE 1
PVDF	POLYVINYLIDENE FLUORIDE
PAR	POLY-ADP RIBOSYLATION
RR	RIBONUCLEOTIDE REDUCTASE
ROI	REGION OF INTEREST
Rx	RECEIVER HEAD
RPA	REPLICATION PROTEIN A
SDS-PAGE	SODIUM DODECYL SULPHATE- POLYACRYLAMIDE GEL ELECTROPHORESIS
TACE	TRANS-ARTERIAL CHEMOEMBOLIZATION
Tx	TRANSMISSION HEAD

1. INTRODUCTION

1.1 Hepatocellular carcinoma – an emerging health problem

Primary hepatocellular carcinoma (HCC) is an aggressive disease. Globally, about one million new cases of HCC are diagnosed each year with an identical cause-specific mortality rate demonstrating a very high case fatality rate. It is the fifth most common cause of cancer death in men and the ninth most common cause of cancer death in women (1, 2). Invariably, HCC is associated with underlying liver cirrhosis, chronic inflammation and/or infection. About 80% of the patients have chronic Hepatitis B or C infection (3). The incidence of HCC varies across geographic locations, predominantly because of variations in prevalence of Hepatitis B and C infection, alcohol consumption as well as aflatoxin exposure.

In the United States, the incidence of HCC is relatively low with an estimated occurrence of 3.2 per 100,000 (4, 5). It is estimated that approximately 28,000 new cases of HCC will be diagnosed in 2012 with approximately 20,000 deaths (NCI). However, this incidence is gradually rising and is expected to increase in the coming years (4, 5). The rising incidence can be attributed to an aging population, immigrating population from East Asia, non-alcoholic steatohepatitis and a high incidence of hepatitis C from 1960 to 1990 (with a lag time of 20-30 years). Important demographic differences exist between different parts of the world in regards to HCC. For instance, the average age at the time of presentation in sub-Saharan Africa is 33 years while in the rest of the world it is 50 to 60 years (2, 6). In

U.S. the most common risk factors for the development of HCC are hepatitis C infection (5), hepatitis B infection (7), alcohol use and non-alcoholic steatohepatitis (8). In addition to these risk factors, exposure to environmental toxins such as aflatoxin (9), betel nut (10) and contaminated water containing microcystin (11) is commonly observed in East Asia and parts of Africa. A recent study examining a large cohort demonstrated a significant association between saturated fat or red meat consumption and liver cancer (12). In separate studies, type 2 diabetes and metabolic syndrome have been associated with liver cancer (13, 14). This predisposition may be due to underlying non-alcoholic steatohepatitis.

At presentation, patients usually have either advanced liver cancer, liver dysfunction or both. Signs and symptoms develop late in the course of the disease and are mostly indistinguishable from those of underlying liver dysfunction (15). Because of delayed diagnosis, the median survival of untreated advanced liver cancer is 6 to 20 months (16). Most patients die from local disease with uncompensated liver failure as the initiating event.

1.2 Current treatment strategies

The mainstay of curative therapy for patients with HCC is surgical resection (17). The majority of patients at presentation, however, are not eligible for surgery because of underlying liver dysfunction. In early stage HCC (as defined by Milano/Mazzaferro criteria (18)) with poor liver function, liver transplantation is the preferred option. Patients needing liver transplantation are prioritized according to MELD score (19). Even though patients with HCC receive a higher MELD score, the gap between organ demand and supply may require a lag time of several months.

Under these circumstances bridging therapies are often employed with trans-arterial chemoembolization (TACE) being the most common (20). For patients who do not meet the criteria for resection or transplantation but have localized disease, a multitude of local-regional therapies can be used based on availability and local expertise. These include percutaneous ethanol or acetic acid ablation, radiofrequency or microwave ablation, radiotherapy, bland microspheres or radio therapeutic microspheres (21). Patients eligible for these local-regional therapies including resection or transplantation constitute less than 25% of patients diagnosed with HCC. For the remaining 75% of patients therapeutic options are limited.

For patients with multifocal, unresectable or metastatic HCC, systemic therapy is usually recommended. Conventional cytotoxic therapy has been shown to be of minimal benefit in these patients for multiple reasons. Most importantly, HCC is considered a chemo-refractory tumor with high expression of drug resistance genes products including P-glycoprotein, heat shock proteins and mutated tumor suppressor p53 protein (22-24). Patients with HCC do not tolerate chemotherapy well because of underlying liver dysfunction. Since most patients with HCC succumb to their hepatic dysfunction, this limits our ability to study effectiveness of chemotherapy in the context of a clinical trial. Recently however, a multi-kinase inhibitor, sorafenib showed a modest improvement in median overall survival of approximately 3 months making it the new standard of care (25). While this clinical response of a molecularly targeted therapy is encouraging, the benefit afforded to these patients is transient. A major challenge therefore remains in

understanding drug resistance pathways in HCC and exploiting them for developing better therapies.

1.3 Gemcitabine and resistance mechanisms

1.3.1. Clinical use of gemcitabine as a single agent in advanced HCC: Like most other cytotoxic chemotherapies, gemcitabine has shown minimal benefit in patients with advanced HCC. In one phase II study, 28 previously untreated Taiwanese patients with advanced liver cancer not amenable to local-regional therapies received single agent gemcitabine therapy at 1250mg/m²/wk (26). An overall response rate of 17.8% (95% CI, 2.7-32.9%) was noted. There were no complete responses, 25% had stable disease and 57.2% had disease progression. Most patients progressed within 12 weeks of the start of therapy. The authors concluded that the toxicity of gemcitabine was minimal and favor its use despite short-lived benefit. Contrary to these findings, a study on 20 European patients using a similar regimen demonstrated a much lower partial response rate of 5% (27). Confirming the findings of this study a high-dose gemcitabine regimen in 17 European patients failed to yield any objective response. However, stable disease was noted in 47% of patients during the course of therapy (28). In a follow-up study conducted in the USA, 30 patients with advanced HCC received single-agent gemcitabine at 1000mg/m²/wk. Again, no responses were observed, but 30% of patients had stable disease (29). Fixed-dose rate regimens yield higher intracellular drug concentrations with comparable toxicity to single-bolus regimens in several other solid tumors and may be more effective (30). This regimen was tested in a phase II study where a similar cohort of 50 Asian patients was randomized to

receive gemcitabine as a single agent, either as a bolus or on a fixed-dose rate regimen. The authors noted that there was only one partial response in the fixed-dose rate arm with an overall response rate of 2.1% (31). Except one study from Taiwan, all studies demonstrate that gemcitabine even though well tolerated, is ineffective as a single agent in advanced liver cancer regardless of the dose or regimen used.

1.3.2. Clinical use of gemcitabine as combination therapy in advanced HCC:

Several combination regimens consisting of gemcitabine have been used with more encouraging results. Most often gemcitabine has been combined with platinum-based chemotherapy. For instance, a phase II study comprising 34 previously untreated patients with advanced HCC who received gemcitabine and cisplatin demonstrated an overall response rate of 18% (95% CI 8-34%). Most patients (58%) had stable disease. This regimen was also well tolerated despite hepatic dysfunction (32). In a comparable study of 30 patients that employed cisplatin in place of oxaliplatin, a response rate of 20% was observed with stable disease in 43% of the patients (33). In a more recent study bevacizumab, a monoclonal antibody against vascular endothelial growth factor was added to a gemcitabine and oxaliplatin regimen. A response rate similar to prior studies of about 20% was reported, suggesting no added benefit from bevacizumab (34). Gemcitabine has also been used in combination with doxorubicin (35). However in 50 patients evaluated, there was a partial response rate of only 11.4% with stable disease in 44% of the patients. Data from these studies demonstrate that gemcitabine is well tolerated but combination therapies are only slightly more effective in comparison to

single-agent gemcitabine therapy. Moreover, the response rates are low and the benefit is transient, underscoring the need to understand resistance mechanisms to these therapies for better approaches to higher and more sustained responses and ultimately to improve median survival.

1.3.1. Mechanism of action and resistance: Gemcitabine (2', 2' - difluoro 2' - deoxycytidine, dFdC) is nucleoside analogue that is similar to deoxycytosine and is structurally related to its predecessor Ara-C (arabinoside cytosine) that showed potent activity in hematologic malignancies. It is a pro-drug that requires transport into the cells before activation and incorporation. Gemcitabine is taken up by the cells via human nucleotide transporters (hNTs) on the cell membrane (36). Upon internalization, it is phosphorylated by deoxycytidine kinase (dCK) to produce gemcitabine mono-phosphate (dFdCMP), di-phosphate (dFdCDP) and tri-phosphate (dFdCTP) in sequential steps (37). Gemcitabine tri-phosphate is the active drug that is incorporated into the DNA or RNA. Once incorporated into the leading and lagging strand of the DNA during replication, gemcitabine allows incorporation of one additional nucleotide before chain termination (38). This phenomenon called masked chain termination is unique to gemcitabine and is believed to be important in its evasion of excision enzymes. Gemcitabine tri-phosphate has several self-potentiating mechanisms that enhance its cytotoxicity by increasing incorporation into the DNA. For instance, dFdCTP inhibits deoxycytidine mono-phosphate deaminase (dCDA), preventing the degradation of its precursor, dFdCMP (39). More importantly dFdCDP is a potent inhibitor of ribonucleotide reductase (RR), an enzyme required for conversion of nucleotide tri-phosphates

(NTPs) into deoxy-NTPs (dNTPs) (40). By inhibiting dNTP synthesis, gemcitabine decreases competition against its incorporation into the DNA. The mechanisms that lead to cell death after incorporation of gemcitabine in the DNA remain elusive, however, apoptosis has been implicated in certain cell types.

Study of gemcitabine resistance has focused on pathways involving its transport and metabolism or those of apoptosis and survival. *In vitro* studies have demonstrated that cells deficient in equilibrative type nucleotide transporter 1 (hENT1) are highly resistant to gemcitabine (36). This observation is consistent with data from patients where hENT1 expression levels correlate with gemcitabine sensitivity (37). Since, gemcitabine needs to be phosphorylated to become active, it is not surprising to note that lack of dCK activity correlates with resistance to gemcitabine (37). Conversely, a higher expression of dCDA in mononuclear cells was associated with resistance to gemcitabine in a cohort of pancreatic cancer patients (41). Additionally, nucleotidase 1 (5' NT-1) plays an important role in dephosphorylating dFdCTP and its over expression has also been associated with lower activity of gemcitabine in several cell lines (42). The most important self-potential mechanism responsible for sustained effective intracellular concentration of gemcitabine is inhibition of RR (40). In non-small cell lung cancer cell lines and patients, over expression of RR sub-unit 1 (RRM1) was associated with gemcitabine resistance and a worse survival (43-46). RR sub-unit 2 (RRM2) modulates RRM1 enzymatic activity. Expectedly, over expression of RRM2 also contributes to gemcitabine resistance (47). Various pro-survival cell-signaling pathways that are associated with gemcitabine resistance in cell lines or animal

models involve phosphatidylinositol 3-kinase/ Akt pathway (48, 49), increased activation or over-expression of focal adhesion kinase (50), c-Src (51, 52) or c-Met (53). Pathways that trigger apoptosis upon exposure to gemcitabine have also been implicated in sensitivity to gemcitabine. For instance, over-expression of S100A4 inhibits gemcitabine-induced apoptosis by regulating the hypoxia-induced pro-apoptotic gene *BNIP3* (54, 55). In addition, it has been shown that p53-deficient cell lines fail to undergo apoptosis in response to gemcitabine in comparison to wild-type p53 counter parts (56-58). These findings demonstrate a multitude of pathways that are now known to be involved in gemcitabine resistance/ sensitivity.

As yet not much is known about the molecules that detect gemcitabine incorporation into the DNA. It is also unclear what mechanisms are at play in repairing gemcitabine-stalled replication forks and if these mechanisms are important in resistance to gemcitabine. Aberrant mismatched nucleotides are removed from the DNA by 3'-5' exonuclease activity of DNA polymerase ϵ (59). It was demonstrated that dFdCMP residues are difficult to excise from the DNA, in part due to masked-chain termination in comparison with dCMP residues (60). Mismatch repair (MMR) enzymes also repair DNA by removing single base aberrancies. MMR-deficient colon cancer and endometrial cells were found to be more resistant than MMR-proficient parental cell lines implicating MMR pathway in repair of gemcitabine-incorporated DNA (61). Recently, the role of homologous recombination repair (HRR) in restarting stalled replication forks has become clearer. Along that line, *Ewald et al.* studied the role of Mre11-Rad50-Nbs1 (MRN) complex in responding to gemcitabine-induced DNA damage (62). They found that

gemcitabine sensitivity was enhanced in cells deficient in one of several components of the pathway, namely, ataxia telangiectasia mutated (ATM), 3'-5' exonuclease Mre11 and Rad50. These findings provide a platform to further study the role of the HRR pathway in gemcitabine resistance.

1.4 Repair of mammalian stalled replication forks

Error-free replication is required to maintain genomic information with high fidelity. In normal cells, spontaneous blocks in replication can occur and can either lead to a stalled replication fork or a collapsed replication fork (63). A stalled replication fork is an arrested fork that can be restarted at a later time. A collapsed fork occurs when the replication machinery dissociates from the DNA or a double strand break occurs. Collapse of a stalled replication fork occurs typically with prolonged replication blocks (64). While the pathways of fork restart are well characterized in prokaryotes, those pathways do not exist in eukaryotic species raising the possibility of alternative pathways. Recent advances in the field have demonstrated that replication-independent mechanisms are involved. This restart requires regression of the fork into a chicken foot-structure (65). In most cases this replication fork intermediate is sensed by poly (ADP-ribose) polymerase 1 (PARP1). Poly-ADP ribose residues in association with the chromatin recruit Mre11, a 3'-5' exonuclease, for DNA end processing (66). The DNA end processing is essential for loading of Rad51 recombinase on the DNA that forms a RAD51 nucleoprotein filament (67). This complex subsequently catalyzes sister chromatid homology search and strand invasion to complete homologous recombination. This model

explains the observations where fork restart has been observed without the need for generating or occurrence of a double strand break (65).

Since cancer cells undergo proliferation at a faster rate under the influence of oncogenes or lack of tumor suppressors, the occurrence of stalled replication forks is also at a higher rate. Failure to restart stalled replication forks without loss or alteration of genetic information is thought to be an important basis of origin of mutations in cancer (as described by oncogene-induced stress model of genomic instability) (68). However once the malignant transformation has occurred, cancer cells may rely on DNA repair pathways such as HRR to propagate the mutated genome. In support of that model, the most commonly mutated gene in cancer, p53, has been shown to tightly regulate the HRR pathway through transcriptional regulation of Rad51 (69-73). For instance, loss of p53 or mutations in the DNA binding domain of p53, up regulate Rad51 expression, which in turn enhances homology-directed repair. These findings highlight the importance of the HRR pathway in maintenance of replication in cancer cells, perhaps more so than in normal cells. The dependence of cancer cells on homology-directed repair can be further enhanced by treatment with replication inhibitors. Many replication inhibitors are already in use in the clinic including hydroxyurea and nucleoside analogues. It has been clearly demonstrated that cells treated with replication inhibitors exhibit pronounced activation of HRR and that this pathway is essential for survival during recovery from stalled replication forks (67). The role of HRR in recovery from nucleoside analogue-stalled replication forks has not been studied specifically. At

least one report suggests localization of HRR pathway proteins to sites of gemcitabine-stalled replication forks (62).

1.5 Thermolabile targets in homologous recombination pathway

Hyperthermia involves raising the temperature of cells, tissues or organs above normal and has been used in the treatment of cancers for more than a century. The earliest observations from Busch demonstrated regression of a sarcoma by fever resulting from erysipelas (74). Later Coley purposely administered the bacterial toxins from *Streptococcus* group A (etiological agent of erysipelas) to reproduce these effects. A variety of cellular and biological processes in cancer cells are preferentially affected by hyperthermia (41-43°C) that may explain the effects observed by Coley. Of these, effects of hyperthermia on DNA replication and repair have been of most interest and form the rational basis of synergy between chemoradiation and hyperthermia.

The seminal observation that implicates the HRR pathway in hyperthermia-related cell death was that cancer cells are most sensitive to hyperthermia during late S and G2 phase of the cell cycle (75). This finding implied that hyperthermia must affect proteins involved in synthesis of DNA and/ or DNA repair. Even though the involvement of the HRR pathway in repair of stalled replication forks has only recently become clear, the thermal effects on the proteins in this pathway have already been observed in the context of DNA double strand break repair as described below.

1.5.1 PARP-1 and hyperthermia: PARP-1 has various cellular functions including modulation of chromatin, transcription and single-strand DNA repair.

Recently, PARP-1 has been implicated in repair of hydroxyurea-stalled replication forks as a sensor upstream of several repair proteins. It has been shown that PARP-1 enzymatic activity is inhibited by hyperthermia (76, 77). This result is mainly due to sumoylation and subsequent ubiquitination of PARP1 upon heat shock. Degradation of PARP1 in this fashion is important in the transcriptional regulation of heat shock protein 70. It was found that in heat shocked rat livers, PARP-1 increases in the insoluble nuclear matrix fraction while it decreases from the soluble fraction of the nucleus (76). This is associated with decreased PARP-1 enzymatic activity. The authors concluded that hyperthermia destabilizes PARP-1 and when denatured, PARP-1 has a higher affinity for the nuclear matrix.

1.5.2 MRN-complex and hyperthermia: This complex is composed of two enzymes Rad50 and Mre11, and one protein with catalytic function Nbs1. These proteins rapidly localize to ionizing radiation-induced double strand breaks where this complex primarily performs DNA end processing before repair. Mre11 is the main excision enzyme with 3'-5' exonuclease activity as well as endonuclease activity. Rad50 can phosphorylate Mre11 and enhance its exonuclease activity while Nbs1 binding enhances endonucleolytic activities of Mre11. Several prior studies have evaluated the effects of heat shock on the functions of the MRN complex. Zhu *et al.* heated U-1 human melanoma cells and HeLa cells for 15 min at 45.5°C and noted translocation of MRN complexes from the nucleus to the cytoplasm (78). This effect lasted 7 hours with only partial recovery of Mre11 and Rad50 levels in the nucleus. A follow up study by the same group administered an equitoxic thermal dose of 42.5°C for 2 hours and found similar patterns of

translocation, however the translocation was enhanced by up to two-fold. It was further shown that administering leptomycin B, an inhibitor of nuclear exporter CRM1, inhibits this translocation suggesting involvement of an active process (79). In a later study, the same group demonstrated that hyperthermia inhibits localization of MRN complex proteins to sites of ionizing radiation-induced double strand breaks and speculated that this may be related to heat-mediated conformational changes in the structure of these proteins (80). The recovery of MRN complex foci took up to 48 hours after heat shock. A more recent study by the same group failed to show that the translocation of MRN complex proteins is important in heat radiosensitization but implicated thermal denaturation of Mre11 in lack of MRN complex formation and subsequent heat radiosensitization (81). They further demonstrated inhibition of 3'-5' exonuclease activity of Mre11 and its increased association with heat shock protein 70 providing evidence of thermal denaturation. These findings implicate Mre11 to be the key target of heat radiosensitization.

1.5.3 BRCA proteins and hyperthermia: The role of BRCA2 in repair of double strand breaks by HRR is well characterized where it mediates Rad51 nucleoprotein filament formation. The role of BRCA2 in repair of stalled replication forks is more complex however. In addition to assisting homology-directed repair, BRCA2 inhibits exonucleolytic degradation of nascent strands at stalled replication forks and keeps end processing by Mre11 3'-5' exonuclease in check (82). Enhanced nucleolytic degradation by Mre11 in the absence of BRCA2 was found to increase chromosomal aberrations without a decrease in survival in cancer cells. Krawczyk *et al.*, while investigating the effects of hyperthermia on HRR of double-

strand breaks demonstrated that thermal radiosensitization is mediated through thermal degradation of BRCA2 downstream of Mre11 (83). Contradictory to prior reports, they found no effects on Mre11 or on the formation of MRN complex. This result could be explained on the basis of lower thermal dose administered in these experiments and may suggest that BRCA2 is more sensitive to thermal effects than Mre11. Degradation of BRCA1 after heat shock has been reported, however, its role in repair of stalled replication forks is uncertain (84).

1.6 Hypothesis and specific aims

The studies mentioned above demonstrate that the main cytotoxic effect of gemcitabine is mediated through its incorporation into the DNA and subsequent stalling of replication fork progression. It is also known that the HRR pathway is the main pathway involved in the repair of stalled replication forks and component proteins of this pathway have been shown to respond to gemcitabine-stalled replication forks. Finally, a profound effect of mild to moderate hyperthermia on several of the key components of the HRR pathway has been demonstrated.

It is not known, however, if HRR of stalled replication forks is a significant mechanism that contributes to chemoresistance of gemcitabine. The effects of hyperthermia on repair of stalled replication forks also remain to be elucidated.

We hypothesize that **mild to moderate hyperthermia can inhibit homologous recombination after gemcitabine-stalled replication forks by its effects on key components of the HRR pathway, hence contributing to chemosensitivity.** Our specific aims are as follows:

Specific aim 1: To identify thermo-labile proteins in the HRR pathway as putative targets of thermal chemosensitization

Specific aim 2: To assess gemcitabine chemosensitization by hyperthermia-induced inhibition of HRR in hepatocellular carcinoma cell lines *in vitro*.

Specific aim 3: To assess anti-tumor activity of gemcitabine with and without non-invasive radiofrequency field-induced hyperthermia in murine orthotopic xenografts of primary hepatocellular carcinoma.

2. Materials and methods

2.1 Cell lines, reagents and transfection

2.1.1. Cell Culture: All cell lines (Hep3B, HepG2 and SNU449) were purchased from American Type Culture Collection (ATCC, Manassas, VA) and maintained according to the supplier's protocol. Media i.e. RPMI-1640 (for SNU449) or MEM (for HepG2 or Hep3B) was supplemented with 10% (v/v) fetal bovine serum. Additional supplementation for Hep3B culture media was performed with sodium pyruvate and non-essential amino acids. Cells were cultured in T-75 or T-150 tissue culture flasks (Corning Inc., Corning, NY). For each cell line short tandem repeat fingerprint was confirmed by the Cell Line Characterization Core Service (M. D. Anderson Cancer Center, Houston, TX) within one year of all experiments. All media and supplements were purchased from Gibco (Life technologies, Grand Island, NY). The cells were passaged approximately every three to five days before reaching confluency. Media was replaced every three days.

2.1.2 Cell Counting: Before each experiment cells were counted. For clonogenic viability assays cells were counted using a hemocytometer and trypan blue staining as described in detail later. For all other assays, counting was performed using a cellometer (Nexcelom Bioscience, Lawrence, MA). First, cells were trypsinized, washed with and re-suspended in PBS. Approximately 20 μ l of cell suspension was diluted 1:1 with trypan blue solution. Of the 40 μ l, 20 μ l was loaded on a disposable counting chamber (Nexcelom Bioscience, Lawrence, MA). The

chamber slide was placed in the cellometer and viable cell counts were noted. For all experiments viability was recorded to be greater than 90%.

2.1.3 Reagents, antibodies and culture plates: All reagents were purchased from Sigma Aldrich (Sigma-Aldrich Corp, St. Louis, MO) unless otherwise stated. Phosphate buffered saline was acquired from the surgical oncology core media facility (M.D. Anderson Cancer Center, Houston, TX). Bromodeoxyuridine (BrdU) was purchased from BD (BD Pharmingen, San Diego, CA). All experimental setups required 6-well or 12-well culture plates purchased from Corning Inc. (Corning, NY).

For fluorescence microscopy, the following primary antibodies were used; rabbit anti-PAR (Trevigen, Gaithersburg, MD), rat anti-RPA32 (4E4, Cell Signaling, Danvers, MA), rabbit anti-Mre11 (GenTex, San Antonio, TX), rabbit anti-rad51 (H-92, Santa Cruz biotechnology, Santa Cruz, CA), mouse anti- γ H2AX (Upstate-Millipore, Billerica, MA), rat anti-BrdU (BU1/75[ICR1], Abcam, Cambridge, MA). Primary antibodies were detected using the following secondary antibodies; Alex Fluor 488 conjugated donkey anti-rat, Alex Fluor 546 conjugated donkey anti-mouse and Alex Fluor 647 conjugated donkey anti-rabbit antibodies (Invitrogen, Grand Island, NY).

For western blot analysis, the following antibodies were used; mouse anti-PARP (Trevigen, Gaithersburg, MD), rabbit anti-NBS1 (Cell Signaling, Danvers, MA), rabbit anti-Rad50 (Cell Signaling, Danvers, MA), rabbit anti-mre11 (Gentex, San Antonio, TX), rabbit anti-rad51 (H-92, Santa Cruz biotechnology, Santa Cruz, CA), mouse anti-p53 (DO-1, Santa Cruz biotechnology, Santa Cruz, CA), rabbit anti-BRCA2 (Calbiochem, Billerica, MA). Primary antibodies were detected using

HRP-linked goat anti-rabbit or goat anti-mouse antibodies (Jackson ImmunoResearch, West Grove, PA)

For colorimetric-based immunohistochemistry, mouse anti-human Ki67 (M7240, Dako, Carpinteria, CA), rabbit anti-cleaved caspase 3 (Asp175, Cell Signaling, Danvers, MA) and rabbit anti-LC3B (Cell Signaling, Danvers, MA) were used

2.1.4 Transfection: Two transfections were performed. First, Hep3B and HepG2 cells were transfected to express GFP and luciferase to facilitate *in vivo* detection of xenografts. Renilla luciferase containing plasmid pRL-TK (Promega, Madison, WI) was modified by adding a GFP sequence. This recombinant plasmid was transfected into NIH 293T cells to generate a lentivirus vector containing the plasmid. This lentivirus was then used to infect Hep3B and HepG2 cell lines. GFP/Luc-transduced stable cells lines were obtained by sorting GFP-positive cells using FACScan (BD biosciences, Boston, MA)

For generating an Mre11-knockdown cell line, we used GPIZ lentiviral shRNA (Open biosystems, Lafayette, CO) according to the supplied protocol. In order to generate lentivirus, Hep3B cells were transfected in separate experiments with three random clones from shRNA library against Mre11 or a control shRNA together with a packaging plasmid (Trans-lentiviral packaging system, Open biosystems, Lafayette, CO) using lipofectamine 2000 (Invitrogen, Life technologies, Grand Island, NY). Approximately 72 hours later, cells were observed under a microscope to express GFP, which is a marker of expression of shRNA against Mre11. Relative mre11 knockdown was confirmed by western blot analysis.

2.2 Protein electrophoresis and immunoblotting

Approximately 200,000 cells were plated in 60mm cell culture plates. Cells formed sub-confluent monolayers. The cells were exposed to moderate hyperthermia in an incubator at 42.5°C for 2 hours and cell lysates were prepared for western blotting before and at 0, 1, 4 and 24-hours after hyperthermia exposure to evaluate the relative levels of various proteins. For preparation of whole cell lysates, media was removed and cells were washed with PBS. Cell lysis buffer (150mM NaCl, 1% NP-40, 0.5% sodium deoxycholate, 0.1% SDS, 50mM Tris, pH 8.0, one mini protease inhibitor/ 10ml tablet Rosche # 11 836 153001) was added on ice and lysed cells were collected after gentle scraping and mixed on ice for 30min. The lysates were spun at 15000 RPM for 10 min at 4°C. The supernatant was collected and stored at -80°C before electrophoresis.

Protein concentrations were measured using Bradford assay (Fischer scientific, Pittsburgh, PA) with bovine serum albumin as the standard curve, according to manufacturer's instructions. The samples were loaded at 20-40 µg/well in a gel using a denaturing sodium dodecyl sulphate- polyacrylamide gel electrophoresis (SDS-PAGE) system. Electrophoresed proteins were transferred onto a polyvinylidene fluoride (PVDF) membrane overnight on ice. The transferred proteins were probed using a specific antibody against each protein of interest. The primary antibody was detected using a horseradish peroxidase (HRP)-conjugated secondary antibody. HRP-conjugated secondary antibody was detected using an Amersham ECL detection system (GE Health Care Biosciences, Pittsburgh, PA).

For BRCA 2 detection, cell lysates were prepared as for other proteins. However, NuPAGE large protein blotting kit was used that utilizes a 3-8% tris-acetate gradient gel allowing better resolution of larger proteins.

2.3 Immunocytochemistry

For immunocytochemistry assay, indirect immunofluorescence approach was used. Circular #1.5 cover slips (Electron microscopy sciences, Hatfield, PA) were placed in 12-well plates and sterilized using a 20-minute UV exposure. Cells from an exponentially growing culture were counted and approximately 50,000 cells were seeded in each well of a 12-well plate. Adherent sub-confluent monolayers were observed growing on the cover slip 24 hours later. At this point cells were exposed to various treatment conditions as described in the results section. At the end of treatment, immunolabeling of proteins being studied was performed. Cells were fixed, permeabilized, blocked, labeled with primary antibody and then with secondary antibody in consecutive steps. Between each step cells were washed with PBS three times for 5 minutes each time on a leveled shaker at 50 RPM. Cells were fixed with 1% paraformaldehyde in PBS (w/v) for 30 minutes. Permeabilization was performed using 0.3 % (v/v) Triton-100 and 0.125 % (w/v) CHAPS (3-[(3-Cholamidopropyl) dimethylammonio]-1-propanesulfonate) dissolved in PBS for 15 minutes. Cells were blocked for 1-hour in a 3 % (w/v) bovine serum albumin and 1 % (v/v) normal goat serum. Primary and secondary antibodies were diluted in the blocking buffer. Incubation with primary antibody was performed over night at 4°C. Secondary antibody incubations were performed for 2 hours at room temperature. At the end of immunolabeling, 4',6-diamidino-2-phenylindole, DAPI (Molecular

probes, Eugene, OR) was used to counter stain DNA at 1:5000 dilution for 15 minutes. Cover slips were washed one more time with PBS and were mounted on frosted glass slides (Fischer Scientific, Waltham, MA) using Dako mounting media (Dako, Carpinteria, CA).

The slides were sealed with a conventional nail polish hardener and stored at 4°C until imaging. For confocal imaging Fluoview - FV1000 Olympus Confocal Microscope (Center Valley, PA) was used. Images were acquired using a 60x (NA1.6, oil) or 100x (NA1.3, oil) objective at an X-Y resolution of 100nm and a Z-stack resolution of ~800nm. Samples were excited using an incident LD laser at 405nm (50mW, 5% power) for DAPI, 559nm (15mW, 20%) for Alex Fluor 546, and 635nm (20mW, 20% power) for Alex Fluor 647. Capture resolution was set at twice the optical resolution and Kallman averaging was set at 2 for enhanced signal to noise ratio. Images were acquired sequentially to minimize cross contamination from multiple emission spectra. Exposure settings were set to maximize dynamic range initially and then kept constant across multiple samples to allow quantitative comparisons.

Acquired images were processed in Slidebook (version 5.0, Intelligent Imaging Innovations, Inc., Denver, CO). Nuclei were identified using the DAPI channel and the areas were converted to regions of interest (ROI). Signals in these ROIs from other channels were used for colocalization analysis. Colocalization thresholds were defined using control images from secondary antibody alone slides such that less than 5% of the pixels exceeded this threshold. Pearson's correlation

was used as an index of colocalization of pixels with intensity above the background threshold.

2.4 Clonogenic assays

Clonogenic assay estimates single-cell reproductive viability by measuring the ability of a single cell to form a colony of 50 cells or more. Clonogenic assay in this study was performed as described previously (85). Briefly, cancer cells from an exponentially growing, sub-confluent culture were trypsinized and harvested. Approximately 200 cells were counted and plated in each well of a 6-well plate. Approximately 12 hours later the cells were adherent and treatment conditions were introduced as described in the results section. After varying treatments, media was replaced and cells were allowed 14 days to form colonies. Subsequently, the media was aspirated and cells were washed with PBS once. Colonies were then fixed with glutaraldehyde (6.0% v/v) and stained with crystal violet (0.5% w/v) for 30 minutes on a leveled shaker at 50 RPM. The fixation and staining solution was then aspirated and the 6-well plates were air-dried after gentle rinsing with tap water. The number of colonies in each well was counted using a colony counting grid. We found that early passage HepG2 failed to form colonies using standard condition or by using pre-conditioned media from the exponentially growing HepG2 culture. Therefore clonogenic assay on HepG2 cells could not be performed.

2.5 Cell cycle analysis

For cell cycle analysis a BrdU-labeling protocol was used to identify cells in S-phase of the cell cycle accurately. Cells were harvested from an exponentially growing culture as described for other experiments and seeded in 6-well plates,

approximately 150,000 cells per well. After 24-hours adherent sub-confluent monolayers were noted and cells were exposed to various experimental conditions. At the end of the treatments, cells were washed and sampled at various time points to study the progression of the cell cycle in time. One hour before each time point, cells were pulsed with BrdU (10 μ M) for 1 hour. BrdU gets incorporated in the DNA of cells in S-phase along with other nucleotides and can be detected using a mouse FITC conjugated anti-BrdU antibody. A BrdU Flow Kit (BD Pharmingen, San Diego, CA) was used according to the supplied instructions without modifications. For counterstaining of DNA content, cells were incubated with 7-amino-actinomycin D (7-AAD) supplied with the kit, on ice for 20 minutes before analysis on a BD LSR II flowcytometer (BD biosciences San Jose, CA).

Single cell populations were identified using forward and side-scatter profiles. A total of 10,000 events were recorded from a gated single cell population. For 7-AAD fluorescence measurements, SORP YG laser (561nm) was used to excite the cells and emission was recorded through a 630LP filter followed by a 660/20 filter. For FITC fluorescence measurements, SORP blue laser (488nm) was used to excite the cells and emission was recorded through 505LP filter followed by a 525/50 filter. There was no spectral over-lap between the two emission spectra and compensation was not required. Data was analyzed using FlowJo 7.63 (Tree Star, Inc., Ashland, OR)

2.6 Mouse model of hepatocellular carcinoma

For *in vivo* studies, an implanted mouse model of human HCC was generated in CB17SCID mice (Taconic Hudson, NY). Female mice between 4-5

weeks in age were purchased and acclimatized in M.D. Anderson Animal facilities for up to 1 week. All animals were handled, housed and studied in accordance with Institutional Animal Care and Use Committee.

Cultured luciferase and GFP-expression human HCC cell lines (Hep3B and HepG2) were harvested from an exponentially growing culture and washed with PBS. The cells were re-suspended in 3ml PBS and final centrifugation was performed at 1000 RPM for 5 minutes. Supernatant was discarded and the cell pellet was used for implantation. The concentration of cells achieved using this protocol was 160,000 cells per micro liter. The cells were kept on ice and animals were injected within 3-4 hours after final centrifugation.

Before surgery hair was removed from the ventral surface of the abdomen using clippers. Mice were anesthetized using 2.5% isoflurane. The surgical field was sterilized with 70% (v/v) ethanol in water. Mice were placed supine on a heating pad and the surgical site was sterilized using povidone iodine swab sticks. After confirming induction of anesthesia, an approximately 1-cm transverse incision was made in the skin of the upper abdomen slightly left of the midline. Deeper layers of muscle and peritoneum were incised and hemostasis was achieved using silver nitrate chemical cautery sticks. By applying gentle pressure on the lower abdomen and lower chest, the left lobe of the liver was eviscerated. A 10 μ l volume of cells was aspirated (~1.6 million cells) using a Hamilton syringe with an angled 30-gauge-needle tip (point style 4, 30 $^{\circ}$, Hamilton Company, Reno, NV). The needle was advanced ~5mm in to the liver parenchyma of the left lobe and the cells were gently deposited ~2mm underneath the liver capsule such that a bleb of fluid was

observed. The needle was carefully withdrawn and the needle track was immediately compressed with a sterilized cotton Q-tip for ~60seconds. A dab of silver nitrate cautery or super glue was used to ensure hemostasis at the needle site. The liver was returned to the peritoneal cavity. Peritoneum, abdomen and skin were closed in a single layer using stainless steel surgical clips (Harvard Apparatus, Holliston, MA). After surgery the mice were allowed to regain consciousness under a thermal lamp and observed for 30-60 minutes before returning them to the housing. Staples were removed 10-14 days after surgery.

Three weeks after implantation of tumor cells in the liver, bioluminescence measurements were performed. D-Luciferin from firefly (Caliper Life Sciences, Hopkinton, MA) was administered at a dose of 150mg/kg in 100µl intra-peritoneally (i.p.). Animals were anesthetized using 2.5% isoflurane and imaged using Xenogen IVIS-200 (Caliper Life Sciences, Hopkinton, MA) 5 minutes after the injection. The imaging was performed over 2 minutes with a 1x1 binning. Mice that had any bioluminescence activity above background (suggesting the development of tumors) were included in the subsequent study. Based on bioluminescence ~95-99% of mice develop tumors 3 weeks after implantation of cells for both tumor models. While bioluminescence imaging was useful in determining the presence of tumors before the start of the study, the levels of bioluminescence did not correlate with the size of the tumors and hence could not be used to track the growth of tumors during the study.

2.7 Radiofrequency generator setup

A Kanzius non-invasive external RF generator (ThermMed, LLC, Erie, PA) was used for animal hyperthermia exposures. The use of this generator has been described previously (86). The generator operates at an adjustable output power (0-2kW) at a fixed frequency, 13.56 MHz. The generator is connected to a high Q coupling system with a Tx head (focused end-fired antenna circuit) and reciprocal Rx head (as a return for the generator) mounted on a swivel bracket allowing the RF field to be oriented in either a horizontal or vertical direction (Figure 1). The two heads were set at a distance of 3.5 inches apart. The Tx head is covered with a Teflon plate whereas the Rx head has a conducting copper surface to allow grounding of the animals as described later. The coaxial end-fire circuit in the Tx head produces a uniform RF electric field up to 15cm in diameter. The field generated is predominantly electric with minimal magnetic component. We have attempted to measure this electric field previously using a Hewlett Packard Spectrum Analyzer (model 8566B, Agilent, Santa Clara, CA), an isotropic field monitor and a probe (models FM2004 and FP2000, Amplifier Research Inc., Souderton, PA). However, at high power output (>100W) accurate measurements cannot be performed because of heating of the measurement probe itself.

For animal RF field exposures, mice were anesthetized with a cocktail of ketamine (100 mg/kg i.p.) and xyalzine (10 mg/kg i.p.). Hairs were removed from the anterior abdominal wall using clippers. Before administering RF exposures, certain steps were taken to ensure prevention of electrothermal injury. For instance, mice that urinate in the RF field suffer severe burns in the groin region. This is

because urine with high ionic content heats significantly faster than the mouse in an RF-field. By gently pressing on the lower abdomen of the mouse, urine was removed from the bladder before RF exposures. Parts of mouse's body with pointed geometry (paws, limbs, ears, whiskers and tail) accumulate a very high charge at the tips because of an impedance mismatch. As a result mice can suffer intense electrothermal burns at these sites. The experiments were therefore performed after grounding all parts of the mouse's body using a copper tape. A window was created within the copper tape grounding-shield to allow RF exposure to the abdomen (Figure 1). All experiments were performed for a 10-minute duration at 600W power output to be consistent with prior reports in the literature (86).

2.8 Thermal imaging and fiber optic thermography

During RF-field exposure temperature from the abdominal surface of mice was recorded using an infrared thermal camera (FLIR SC 6000, FLIR Systems, Inc., Boston, MA). This non-invasive measurement was performed for all mice to ensure that the surface temperature did not exceed 43°C.

For liver and orthotopic xenograft measurements fiber optic thermography was employed. Fluotemp, a fiber-optic probe (PhotonControl, Burnaby, BC, Canada), 400 microns in diameter with a scientific accuracy of $0.1\pm^{\circ}\text{C}$ was advanced over a 20G, 1-inch needle. The needle was placed in the liver or liver tumor under ultrasound guidance and the probe was advanced into the target organ. Subsequently, the needle was retracted over the fiber-optic probe. This probe was pre-tested for lack of heating in the RF field.

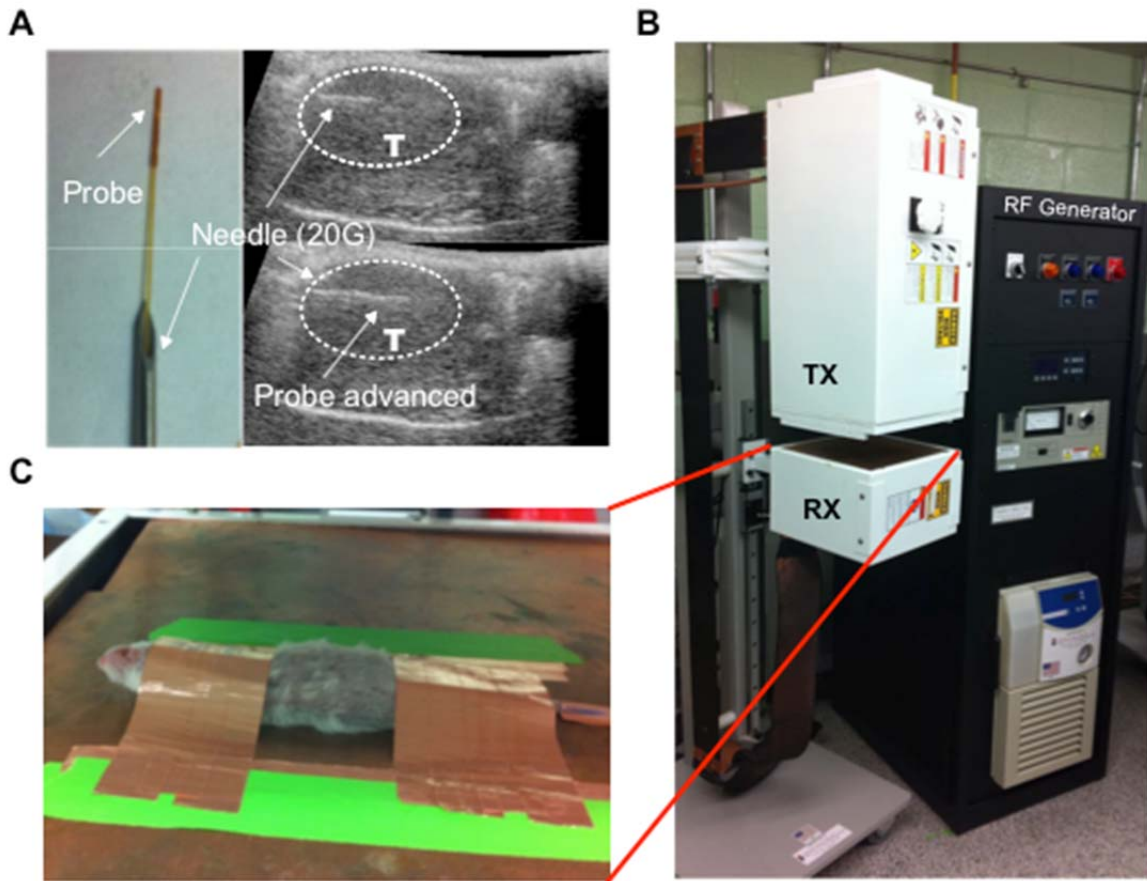


Figure 1. Radiofrequency generator and fiber optic probe placement

Pane A. For fiberoptic thermography, a temperature-sensing probe is placed over a 20G needle. The needle is advanced into the tumor (T) under ultrasound guidance. The probe is then advanced over the needle and the needle is withdrawn.

Pane B. Kanzius 13.56 MHz external RF generator system is shown (black box) that is connected to an end-firing antenna in the transmission head (Tx). A spacing of 3.5 inches exists between the Tx head and the receiver head (Rx)/ ground plate.

Panel C. A CB17 SCID mouse is placed supine on the ground plate of the Rx head. A copper shield made from copper tape is used to ground the mice and prevent electrothermal injury. An abdominal window is created in the middle of the copper shield to allow thermal exposures to the tumor.

2.8 Immunohistochemistry

Tumor tissues harvested at the end of the experiment were fixed in 10% buffered formalin (pH 7.0) for 24 hours and subsequently stored in 70% Ethanol (v/v) before embedding them in paraffin. For immunohistochemistry 5-micron sections were placed on a glass slide and tissue sections were de-paraffinized and rehydrated. Antigen retrieval was performed in citrate buffer at pH 6.0. The slides were placed in Tris-buffer (pH 8.0) before further processing.

For fluorescence immunohistochemistry, a protocol similar to that used for immunocytochemistry (described above) was used with some modifications described here. Tris-buffer was removed and tumor section was encircled using a pap pen (Electron microscopy sciences, Hatfield, PA). For blocking 5% (w/v) BSA and 3 % (v/v) NGS was used instead of 3% BSA and 1% NGS, respectively. Imaging was performed as for immunocytochemistry.

For chromogen-based immunohistochemistry, cleaved caspase-3 (CC-3) and LC3B protein were detected using a rabbit monoclonal antibody, and Ki67 was detected using a mouse monoclonal antibody. Mouse antibody was detected using mouse-on-mouse HRP-Polymer Kit (BioCare Medical, Concord, CA). Rabbit antibody was detected using EnVision+/^{HRP}, rabbit kit (Dako, Carpinteria, CA). The staining was performed on a Dako automated stainer (Dako, Carpinteria, CA). Primary antibody incubation was 30 minutes. The slides were counterstained with hematoxylin and a cover slip was sealed in place. Images were acquired using a multispectral scope (Olympus IX51 featuring a CRi Nuance camera, Hopkinton, MA). Staining was quantified using inFormTM (CRI, Capillary Life Sciences,

Hopkinton, MA), pattern recognition software that subjects multispectral data to machine-learning algorithms for accurate quantification of staining.

2.9 Statistical Analyses

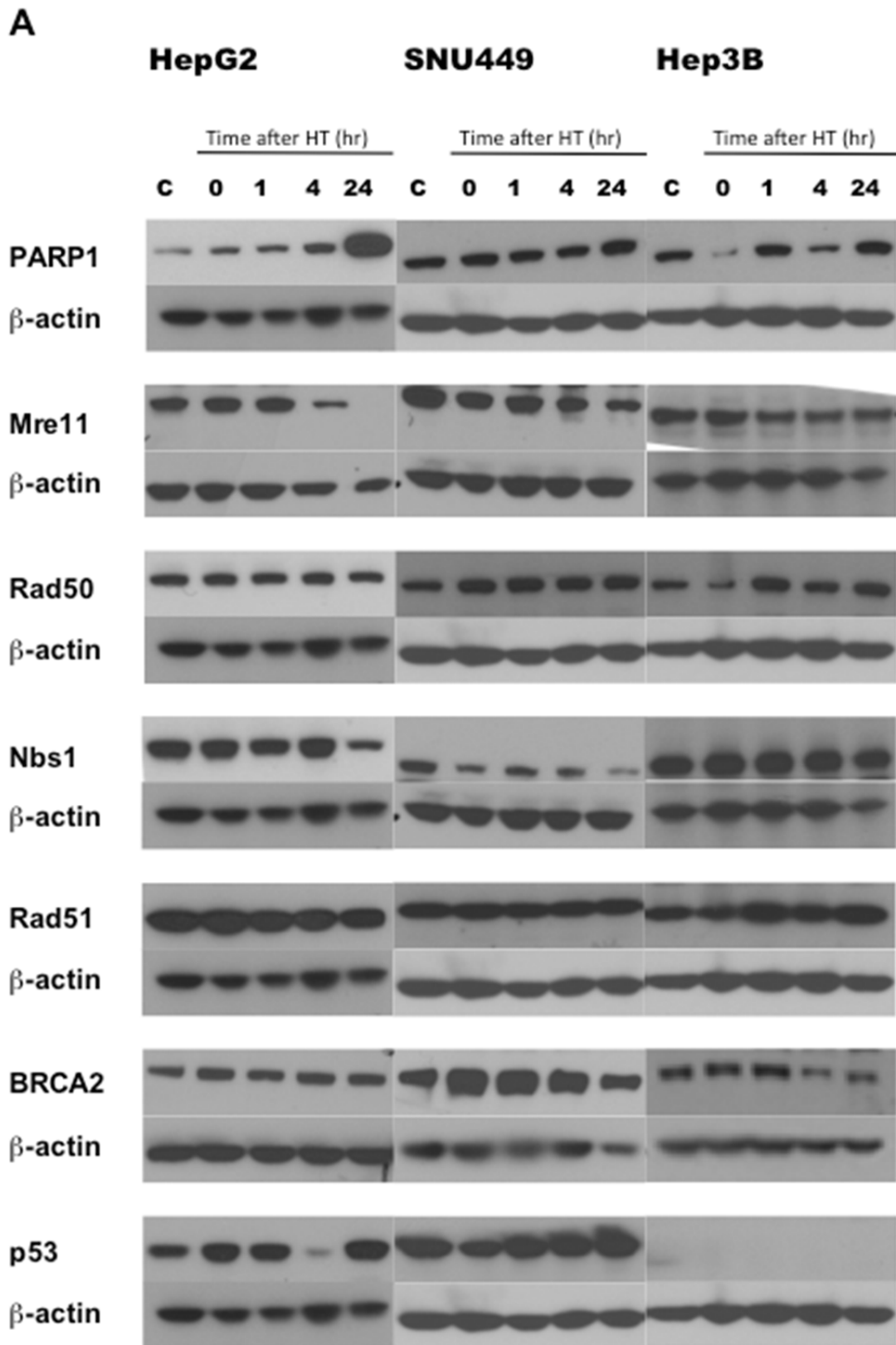
The data were plotted and analyzed in GraphPad Prism (version 5, La Jolla, CA). For data with Gaussian distribution and when comparing two groups, Student's t-test was used. Multiple group data was analyzed using one-way analysis of variance (ANOVA). Where necessary ad-hoc post-tests were performed and the type of test used is reported with the results. For all inferential statistics a p-value <0.05 was considered significant.

3. Results

3.1 Effect of moderate hyperthermia on HRR-pathway proteins

To investigate the effects of moderate hyperthermia on HRR-pathway proteins, we evaluated three cells lines with varying p53 status i.e. Hep3B (p53^{-/-}), HepG2 (p53^{wt/wt}) and SNU449 (p53^{mut/mut}; A161T). Exponentially growing cells in 60mm plates were subjected to hyperthermia at 42.5°C for 2 hours in an incubator with humidified air and 5% CO₂. Protein expression levels were monitored before thermal exposure, immediately after thermal exposure and then over-time at 1 hour, 4 hour and 24-hour intervals, in whole-cell lysates. The data are shown in Figure 2.

The data demonstrate that with moderate hyperthermia exposure, initially there is mild degradation of PARP-1 for Hep3B cells, while there is little or no change for HepG2 and SNU449 cell lines. At 24 hours, however, PARP-1 levels tend to increase (~5-fold) compared to control levels more in HepG2 cells but not in SNU449 or Hep3B cells. Levels of p53, NBS1, Rad50 and Rad51 do not change with thermal exposure in any of the cell lines tested. Interestingly, we find that levels of Mre11 gradually decline after heat shock in all cell lines to less than half of the control levels at 24 hours. This finding is most pronounced for HepG2 cells. It has been previously reported that BRCA2 is an important target of heat radiosensitization (83). We find that the effect of hyperthermia on BRCA2 levels was cell line-dependent. The wt-p53, HepG2 cells and mutant-p53, SNU449 cells demonstrated negligible changes in BRCA2 levels after thermal exposure, however p53-null, Hep3B cells demonstrated a slight decrease in BRCA2 levels.



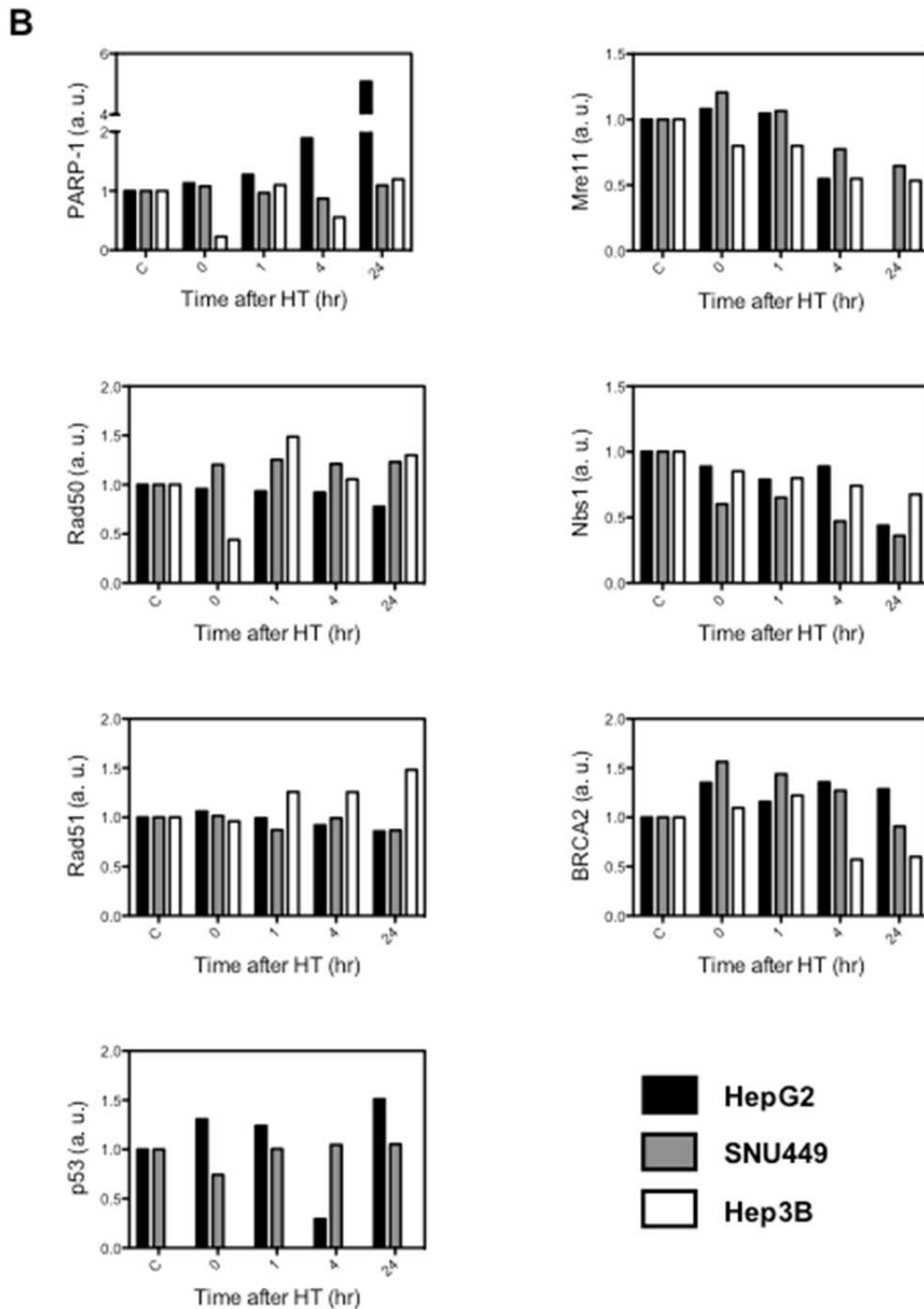


Figure 2. Effect of moderate hyperthermia on HRR-pathway proteins

Three liver cancer cell lines with varying p53 status were subjected to hyperthermia at 42.5°C for 2 hours and levels of proteins monitored over time. C= control, before hyperthermia. (A) Immunoblots, (B) Quantification by densitometry.

3.2 Localization of HRR-pathway proteins to gemcitabine-stalled replication forks

We asked if hyperthermia impairs localization of HRR-pathway proteins to gemcitabine-stalled replication forks. To address that question we first sought to investigate γ H2AX-p as a marker of stalled replication forks. Phosphorylation of γ -H2AX has been observed to occur in association with double-stranded DNA breaks induced by ionizing radiation. Increasing evidence has accumulated since then, demonstrating γ -H2AX phosphorylation to be a sensitive but non-specific marker of a wide-variety of insults to the DNA. For instance, it has previously been reported that γ -H2AX-p foci mark gemcitabine-stalled replication forks without occurrence of dsDNA breaks. It is also known that hyperthermia can induce γ -H2AX foci without detectable damage to the DNA. To evaluate if γ -H2AX foci localize to stalled replication forks, Hep3B cells were pulsed with BrdU for 30 min prior to addition of gemcitabine. We found that almost all γ -H2AX foci localize with BrdU foci confirming its presence at stalled replication forks (Figure 3). Cells that were treated with hyperthermia alone also demonstrated γ -H2AX foci. We find that these foci were significantly fewer ($p < 0.001$) than gemcitabine treated cells. Interestingly, γ -H2AX foci were only found in cells positive for BrdU suggesting specificity for S-phase (Figure 4). Combining hyperthermia immediately followed by gemcitabine treatment did not further increase γ -H2AX foci compared to the gemcitabine alone group. This suggests a common etiology to the origin of γ -H2AX foci with hyperthermia i.e. stalled replication forks. Transient stalling of replication forks is known to occur with hyperthermia based on prior reports (87). If this assumption is correct then

hyperthermia induced- γ -H2AX foci should colocalize with single-stranded DNA that arises as a result of a stalled replication forks. Using replication protein A (RPA) as a marker of single-stranded DNA we found that γ -H2AX foci after hyperthermia exclusively colocalize with RPA foci confirming the nature γ -H2AX phosphorylation after hyperthermia, which was previously not known (Figure 5).

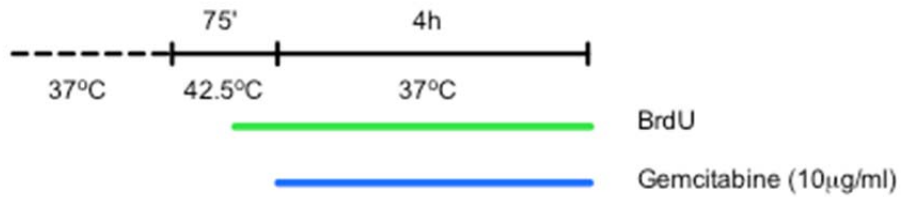
After establishing γ -H2AX foci as a marker of stalled replication forks, we evaluated recruitment of downstream pathway proteins to these sites. We exposed cells to mild hyperthermia at 42.5°C for 75 min followed immediately by a high concentration of gemcitabine (10 μ g/ml). This concentration was chosen to induce maximal stalling of replication forks and hence maximum number of γ -H2AX foci in each cell. It has previously been reported that PARP1 serves as an initial sensor at hydroxyurea-stalled replication forks and catalyzes poly-ADP ribosylation (PAR) at these sites. Localization of PARP1 within the nucleus is diffuse and does not form distinct foci. However, PAR residues can form foci that can be detected using a specific antibody. We found that there was no correlation between PAR staining and γ -H2AX foci (not shown). Furthermore, PAR staining was found to occur in most untreated cells suggesting a high baseline level of PARylation of chromatin.

Stalled replication forks can cause uncoupling between the replication machinery and the double-stranded DNA unwinding helicase. This stalling leads to stretches of single-stranded DNA. Replication protein A (RPA) has a high affinity for single stranded DNA and is important in recruitment of downstream HRR-pathway proteins to stalled replication forks. We find that pre-treatment with hyperthermia does not inhibit localization of RPA to the sites of stalled replication forks (Figure 5,

8). Downstream, RPA recruits proteins of the Mre11-Rad50-Nbs1 (MRN) complex. Localization of the MRN complex to stalled replication forks is essential for HRR. Within this complex, Mre11 is the key effector with known 3'-5' exonuclease as well as 5'-3' endonuclease activity. In particular, Mre11 nucleolytic activity allows loading of Rad51 recombinase by processing DNA ends at stalled replication forks. We note that pre-treatment with mild hyperthermia impairs localization of Mre11 to sites with γ -H2AX foci (Figure 6, 8). This pre-treatment further leads to inhibition of Rad51 loading at stalled replication possibly because of inhibited end processing by Mre11 (Figure 7, 8).

These data demonstrate that hyperthermia alters localization of the HRR-pathway proteins at sites of stalled replication forks. We identify Mre11 as a key thermolabile target of hyperthermia.

A. Experimental design



B.

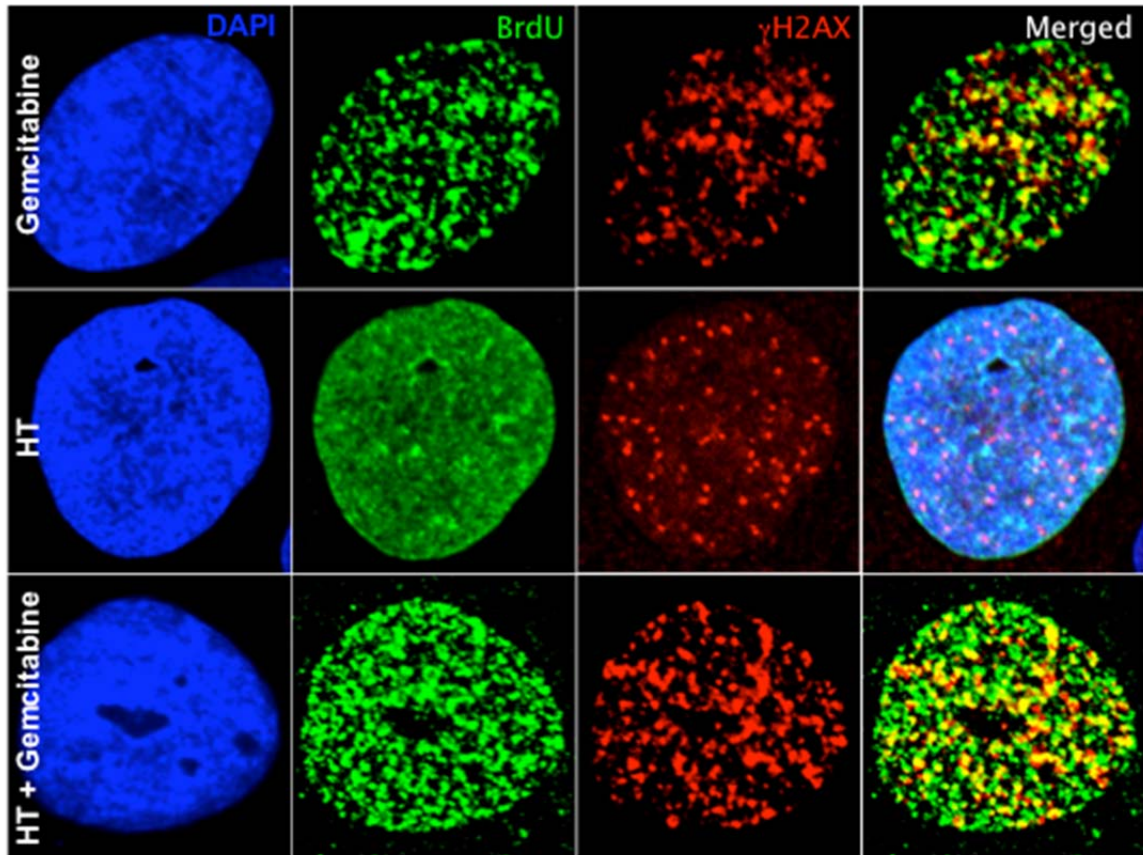
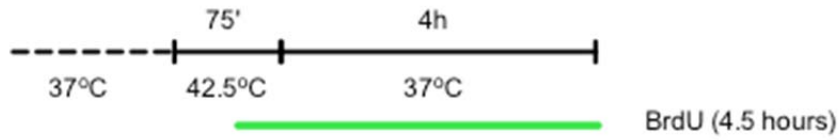


Figure 3. Gemcitabine-stalled replication forks are marked by γ -H2AX foci.

Panel A. Hep3B cells were exposed to hyperthermia and/ or gemcitabine and DNA immediately upstream of stalled replication forks was labeled with BrdU.

Panel B. Distinct foci marking gemcitabine-stalled replication forks are detected by anti-BrdU antibody. γ -H2AX foci colocalize at sites of stalled replication

A. Experimental design



B.

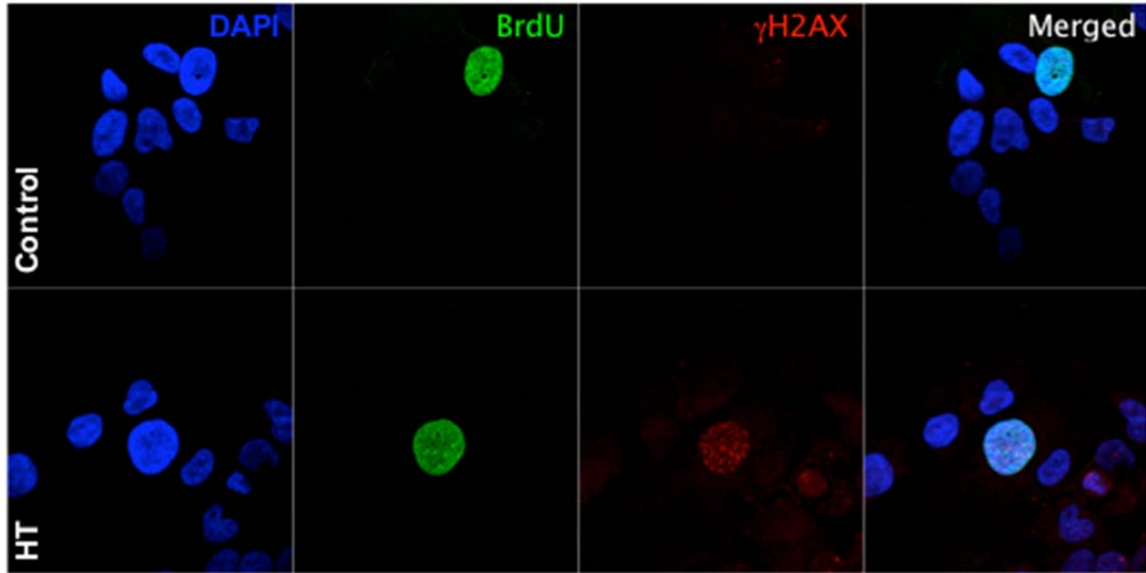
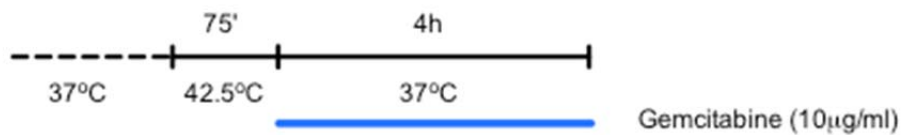


Figure 4. Hyperthermia-induced γ -H2AX foci are S-phase specific

Panel A. S-phase cells were marked using BrdU incorporation over a period of 4.5 hours immediately after hyperthermia

Panel B. It was noted that hyperthermia-induced γ -H2AX foci only occurred in cells staining positive for BrdU (S-phase cells)

A. Experimental design



B.

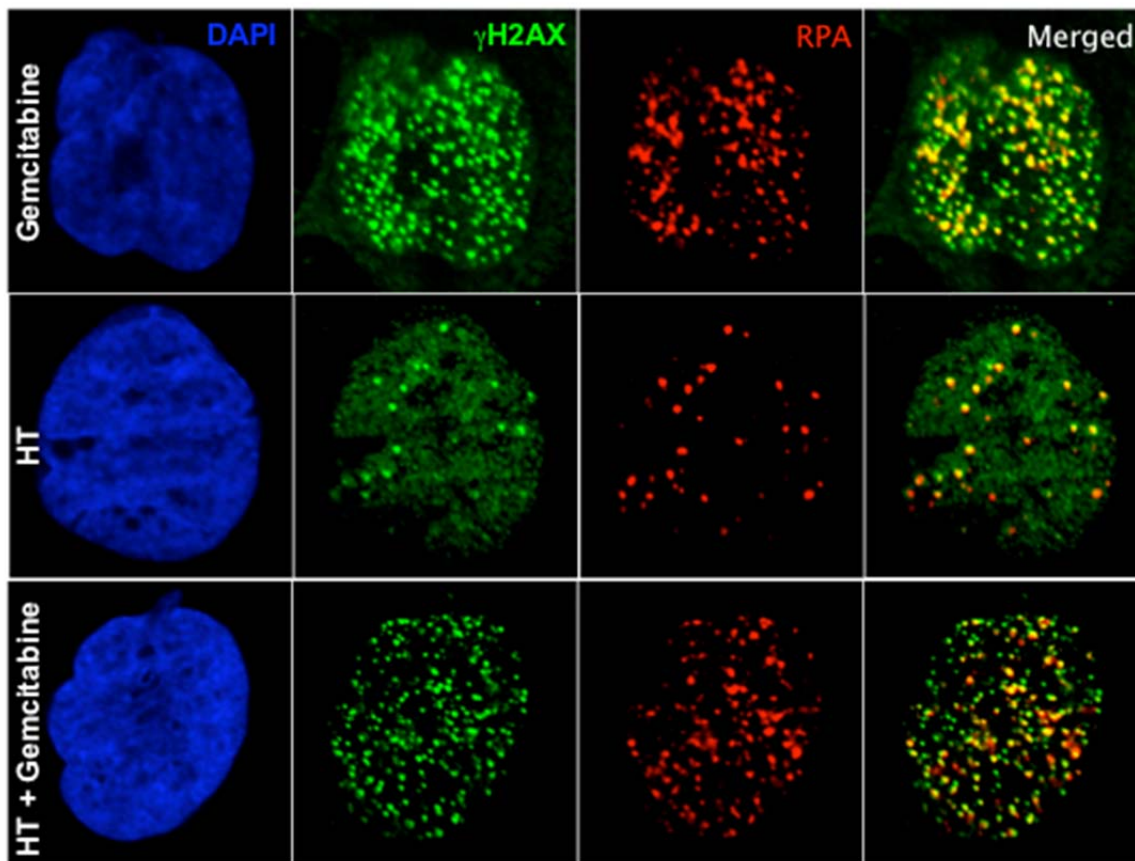
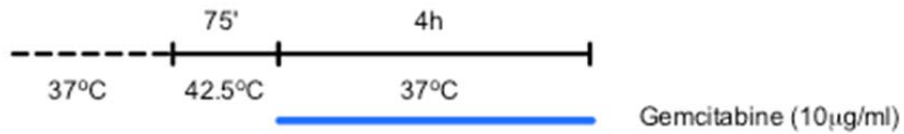


Figure 5. Gemcitabine and hyperthermia-stalled replication forks recruit RPA

Panel A. Hep3B cells were exposed to hyperthermia and/ or gemcitabine

Panel B. RPA colocalizes with γ -H2AX foci in cells treated with gemcitabine, hyperthermia or combination of the two treatments.

A. Experimental design



B.

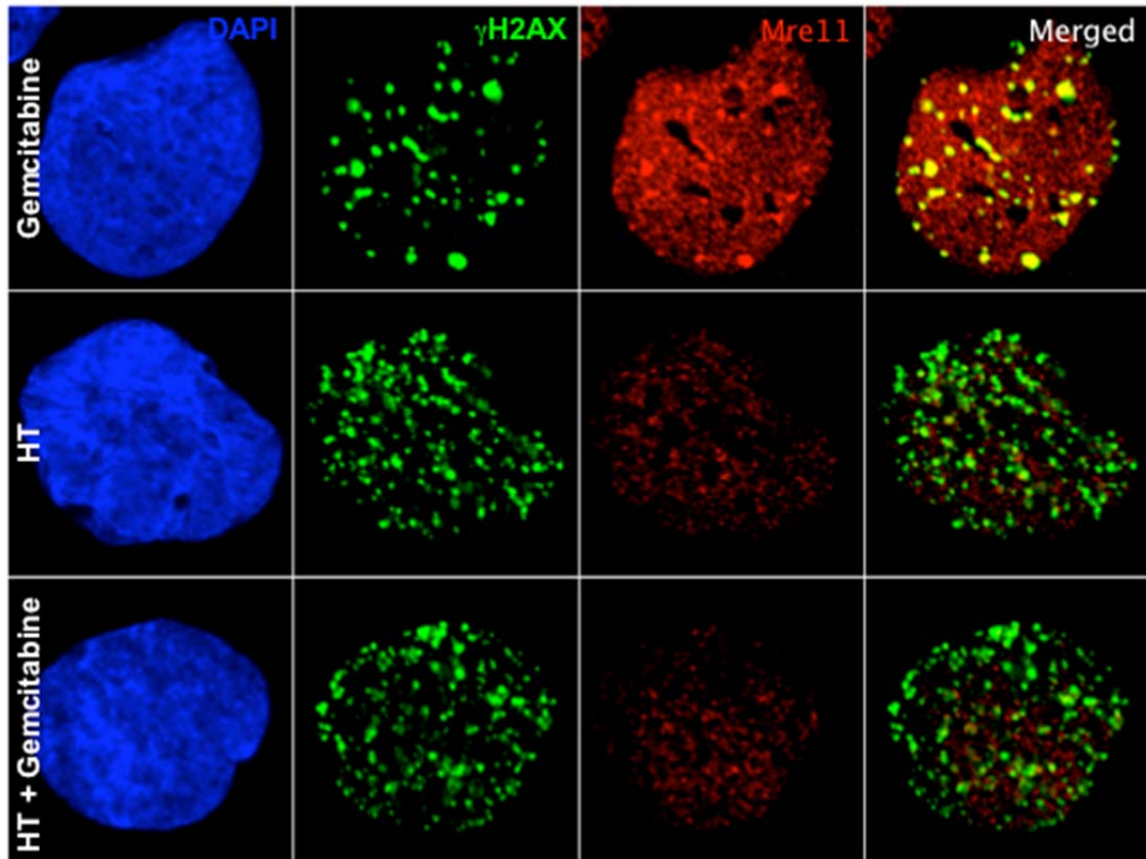
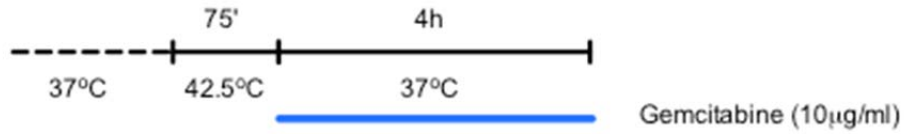


Figure 6. Inhibition of Mre11 recruitment at gemcitabine-stalled replication forks by hyperthermia

Panel A. Hep3B cells were exposed to hyperthermia and/ or gemcitabine

Panel B. Mre11 was recruited at gemcitabine-stalled replication forks. Cells treated with hyperthermia or combination with gemcitabine demonstrated decreased colocalization of Mre11 and γ -H2AX foci.

A. Experimental design



B.

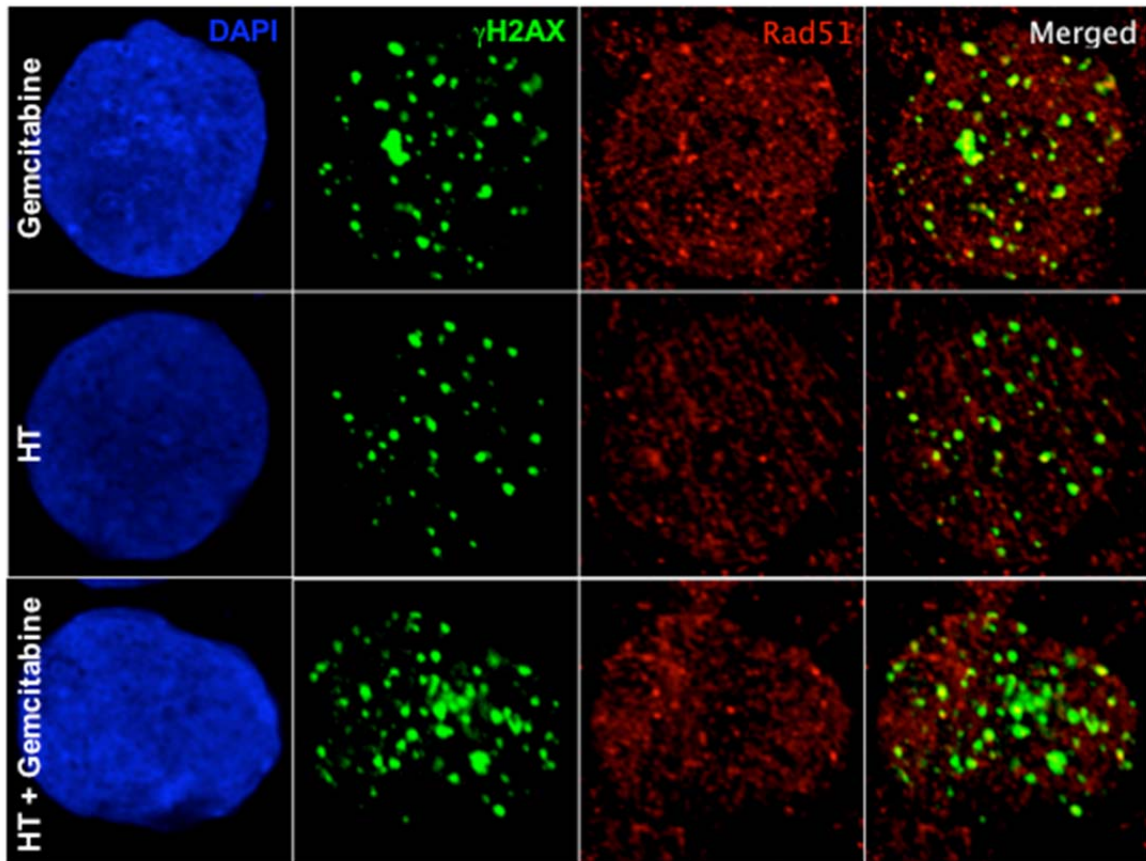


Figure 7. Inhibition of Rad51 recruitment at gemcitabine-stalled replication forks by hyperthermia

Panel A. Hep3B cells were exposed to hyperthermia and/ or gemcitabine

Panel B. Rad51 was recruited at gemcitabine-stalled replication forks. Cells treated with hyperthermia or combination with gemcitabine demonstrated decreased colocalization of Rad51 and γ -H2AX foci.

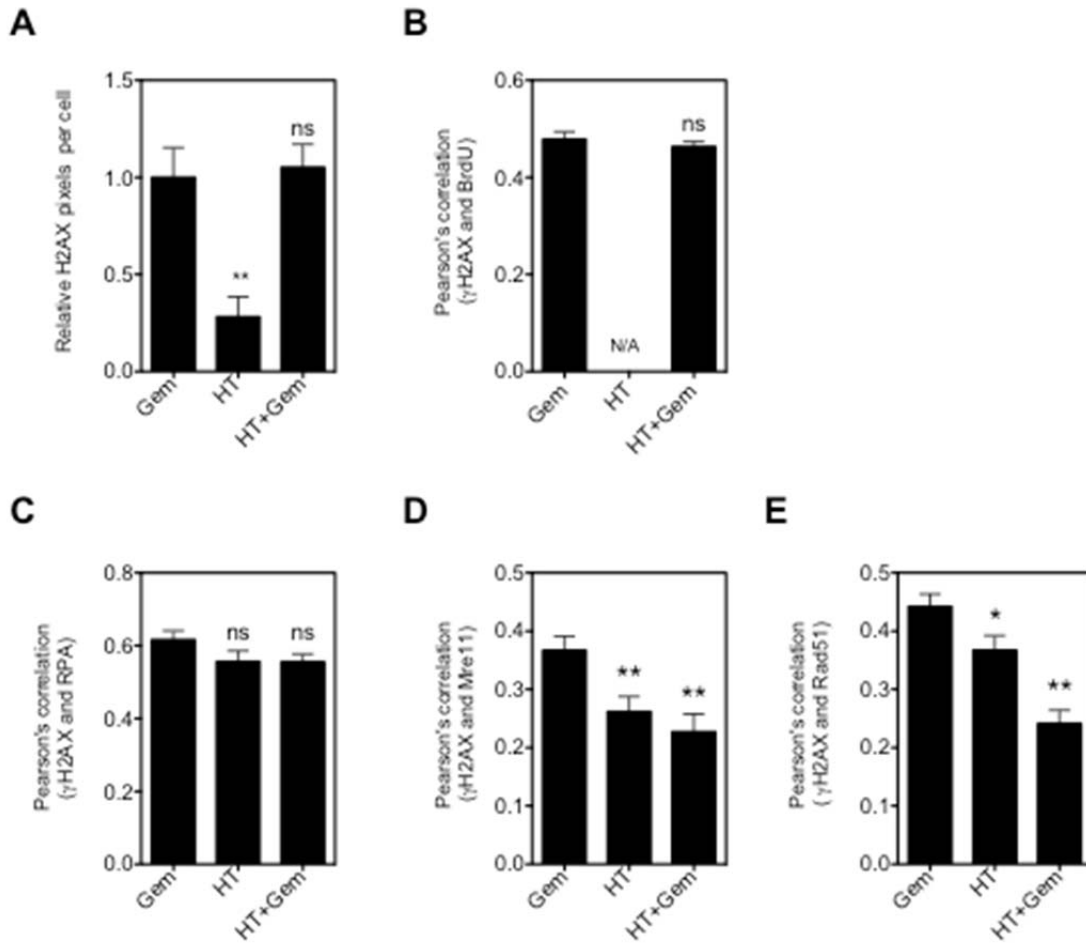


Figure 8. Quantification of data presented in Figure 3-7

*p<0.05, **p<0.01, ns = not significant, N/A = not applicable i.e. Hyperthermia treated cells is not detected as distinct foci and therefore correlation could not be quantified.

3.3 Cell cycle alterations

The data thus far suggest that hyperthermia can alter the expression levels and localization of HRR-pathway proteins. Since stalled replication forks are primarily repaired through recombination-mediated repair, we postulated that hyperthermia would inhibit the repair of gemcitabine-stalled replication forks delaying progression through the cell cycle.

To test this hypothesis, we exposed Hep3B cells to gemcitabine for 24 hours (approximate doubling time of Hep3B cells) at a concentration of 1 μ M. This concentration is comparable to the peak intracellular concentration achieved with clinically used fixed-dose rate regimens (88). Since incorporation of gemcitabine only occurs during S-phase, exposing Hep3B cells for 24 hours ensures incorporation of gemcitabine in all cells. For the last 2 hours of incubation, cells were or were not exposed to hyperthermia at 42.5°C. The cells were washed with PBS and media was replaced to allow recovery of stalled replication forks. Cell cycle progression was analyzed over time (Figure 9A).

We note that a 24-hour incubation with 1 μ M gemcitabine completely halts progression of cells through the cell cycle by activating a G1/S checkpoint (Figure 9B). Once gemcitabine is removed, these cells resume DNA synthesis in 24 hours in a synchronized manner suggesting gemcitabine-induced cell cycle arrest is reversible at clinically relevant concentrations. Interestingly the delay caused by hyperthermia in progression through early and mid S-phase was negligible. We noted however, that gemcitabine followed by hyperthermia-treated cells demonstrate a much slower progression through late-S and G2/M phase compared

to cells treated with gemcitabine alone. This delayed arrest in late-S and G2 phase with normal progression through early and mid S-phase demonstrates the temporal separation of replication and recombination and is further discussed later. We also note that the effect of hyperthermia on repair of stalled replication forks is transient (lasting a few hours) as most cells progress to G0/G1 phase of the cell cycle eventually.

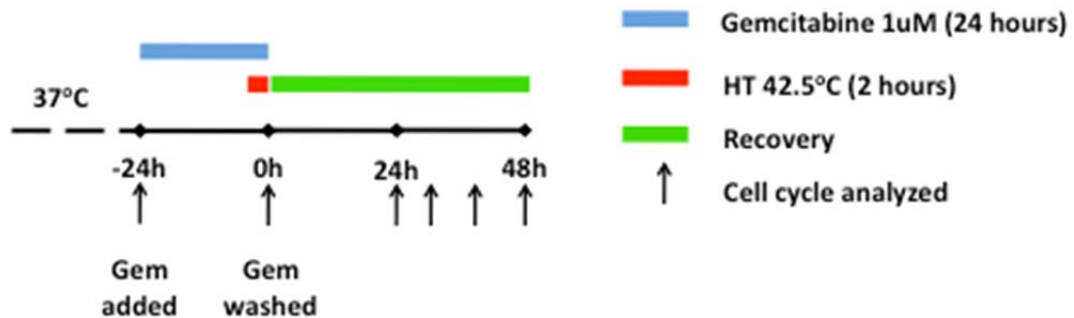
Consistent with prior observations, our data demonstrate a late-S/ G2 arrest when cells are treated with moderate hyperthermia alone (89-92). Although several reports have noted this observation, an explanation of underlying mechanisms has been lacking. Here we find that the duration of G2 arrest is ~39-48 hours. This matches the delay in progression of cells through late-S/ G2 phase after recovery from gemcitabine-stalled replication forks. Since recombination repair predominantly occurs in late-S/ G2 phase, hyperthermia alone may inhibit HRR required for spontaneously arising stalled replication forks. Hence, the data provide a rational explanation of G2 arrest occurring after hyperthermia.

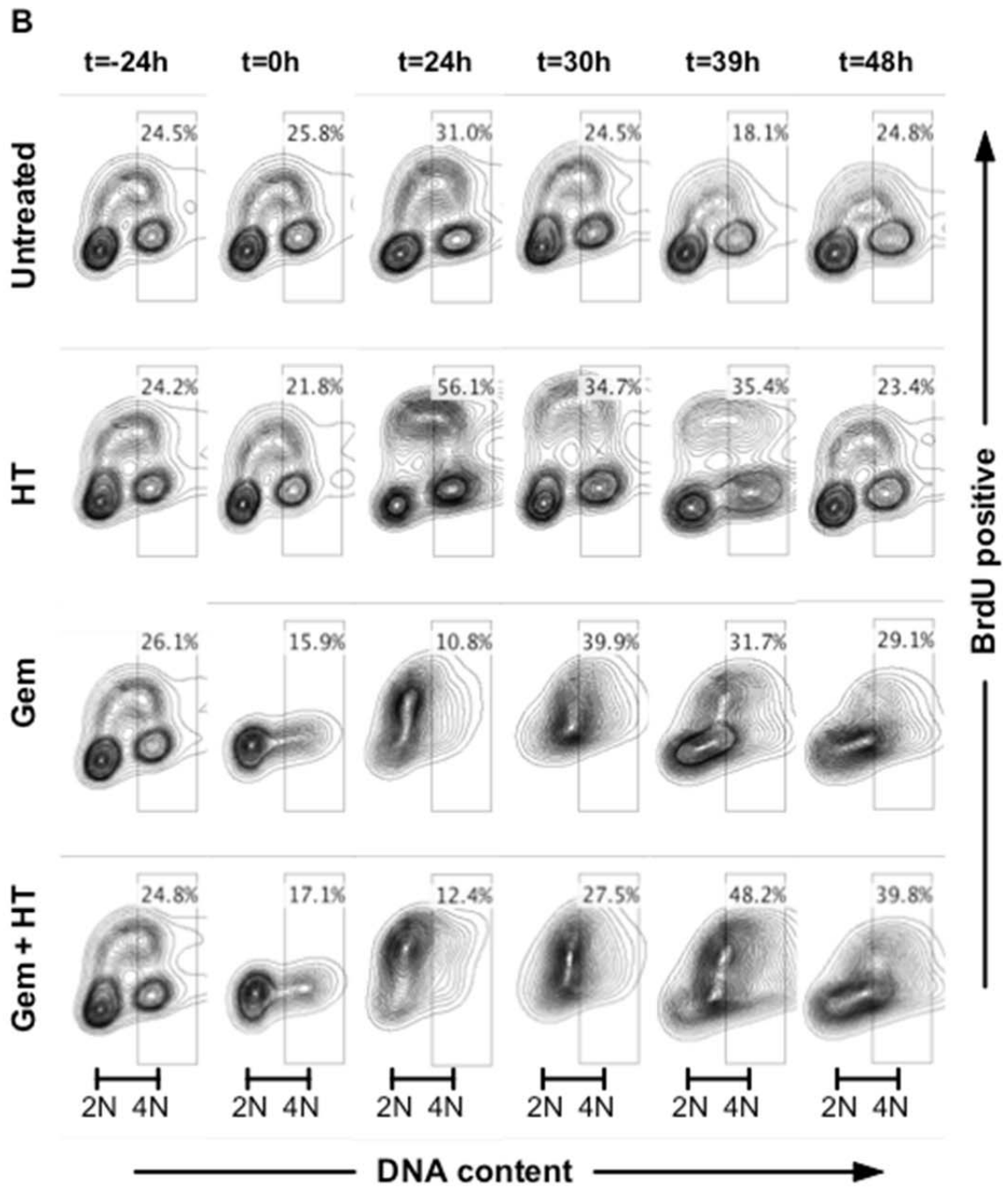
Cancer cells that fail to resolve stalled replication forks demonstrate persistent staining for γ -H2AX phosphorylation sites. We used this strategy to evaluate if gemcitabine treatment followed by hyperthermia would demonstrate persistence of γ -H2AX positive cells in comparison with gemcitabine treatment alone. To test this hypothesis we treated Hep3B cells with gemcitabine (100nM) for 24 hours. For the last 2 hours, cells were treated with or without hyperthermia at 42.5°C. The media was then replaced and cells were allowed to recover from gemcitabine-stalled replication forks. We note that when cells are treated with a

combination of gemcitabine and hyperthermia, γ -H2AX positive cells persist for a longer duration compared to hyperthermia alone or gemcitabine alone treated cells (Figure 9D). Moreover, the resolution of γ -H2AX positivity coincides with the progression of cell cycle observed in the previous experiment.

These experiments demonstrate that hyperthermia significantly alters cell cycle progression by inhibiting post-replication recombination repair and resolution of gemcitabine-stalled replication forks as observed by persistent γ -H2AX staining. We also note that this inhibitory effect is transient lasting with a duration of 48 hours after hyperthermia exposure.

A. Experimental design





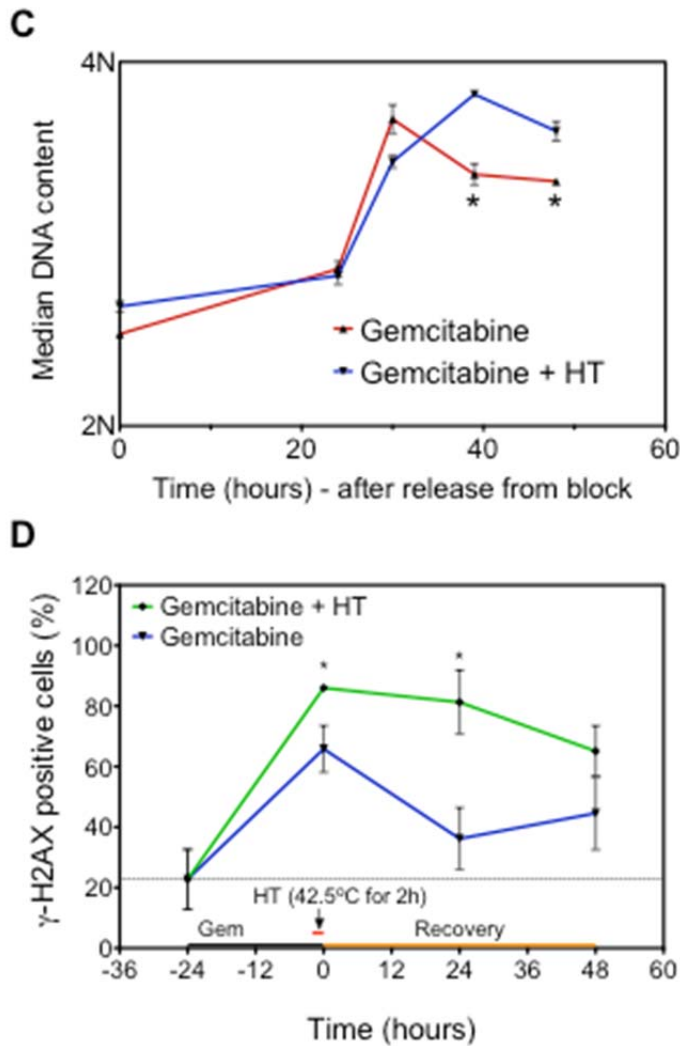


Figure 9. Hyperthermia inhibits post-replication recombination repair at gemcitabine-stalled replication forks.

Panel A. Experimental scheme is presented

Panel B. Cell cycle progression was monitored using flowcytometry in Hep3B cells before after release from gemcitabine-induced G1/S arrest.

Panel C. Median DNA content of Hep3B cells was quantified using flowcytometry after treating them according to the design in Panel A. (* $p < 0.05$)

Panel D. Hep3B cells were treated with gemcitabine +/- hyperthermia and cells positive for γ -H2AX foci in confocal microscopy images were quantified. (* $p < 0.05$)

3.4 Clonogenic survival & viability

Next, we wanted to understand the consequences of pronounced cell cycle alterations and inhibition of stalled replication fork repair by hyperthermia on reproductive viability of cancer cells. Clonogenic assays were performed on null-p53 Hep3B cells and mutant-p53 SNU449 cells after one of two combinations of hyperthermia and gemcitabine in comparison with hyperthermia alone or gemcitabine alone. Of note, WT-p53 HepG2 cells failed to form colonies when plated as single cells for clonogenic assay, precluding further analysis of these cells.

In one combination regimen, Hep3B or SNU449 cells were exposed to gemcitabine for 24 hours and were then subjected to hyperthermia for the final 2 hours at 42.5°C. In a different combination regimen Hep3B or SNU449 cells were exposed to hyperthermia for 2 hours at 42.5°C followed by gemcitabine for 24 hours. The media was replaced at the end of exposures and the colonies were counted after appropriate duration. Figure 10 demonstrates a dose-dependent enhancement of gemcitabine toxicity by moderate hyperthermia in both SNU449 and Hep3B cells irrespective of the dose schedule used. Next we evaluated clonogenic viability at a gemcitabine concentration of 5ng/ml and varied the duration of hyperthermia (30min - 4 hours). The data demonstrate a thermal dose-dependent enhancement in synergistic toxicity of gemcitabine and hyperthermia.

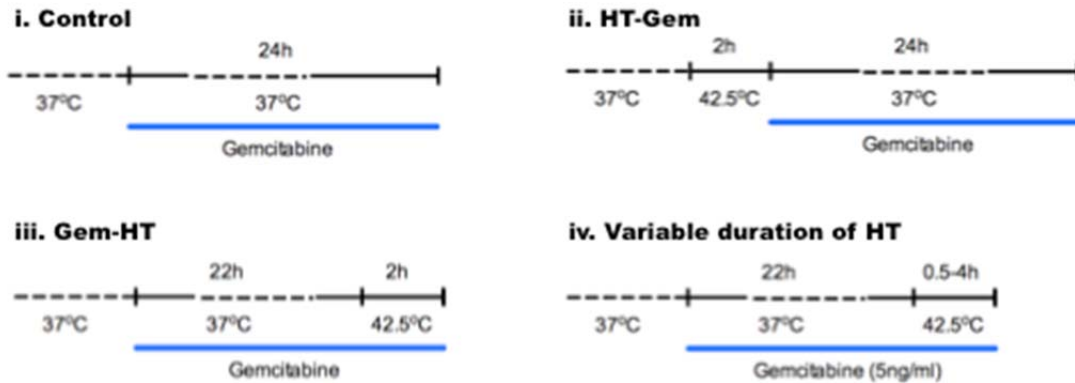
Prior studies conducted as a part of this thesis demonstrated that Mre11 is a key thermolabile target of hyperthermia. We asked if inhibition of Mre11 exonuclease activity by a specific inhibitor, mirin, would result in similar

enhancement of gemcitabine toxicity. The above experiments were repeated with and without a sub-cytotoxic dose of mirin (25 μ M). We found that inhibition of Mre11 exonuclease activity by mirin significantly enhanced gemcitabine-induced clonogenic cell death (Figure 11). Furthermore, addition of hyperthermia did not further enhance this toxicity confirming that thermal enhancement of gemcitabine toxicity is mediated through an Mre11-dependent pathway.

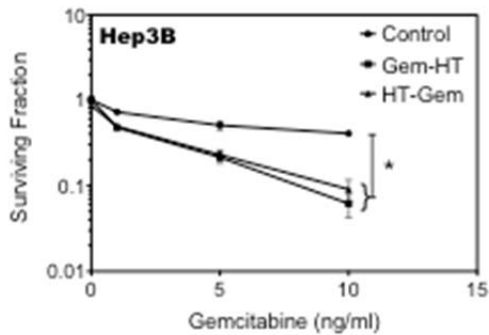
To rule out the possibility of off-target effects of mirin, we developed a partial Mre11 knockdown (shMre11) Hep3B cell line. Hep3B cells with complete knockdown of Mre11 expression were not stable in cell culture. These cells were then treated with or without gemcitabine and with or without hyperthermia. The results are compared to a cell line expressing a non-specific shRNA (shControl) subjected to same experiments. Similar to the results obtained with mirin, we found that shMre11 cell line was more sensitive to gemcitabine in comparison with shControl cell line. Furthermore, thermal enhancement of gemcitabine toxicity was noted for shControl cell line but not with shMre11 cell line.

These data strongly implicate an Mre11-dependent homologous recombination repair pathway in thermal enhancement of gemcitabine-induced cytotoxicity.

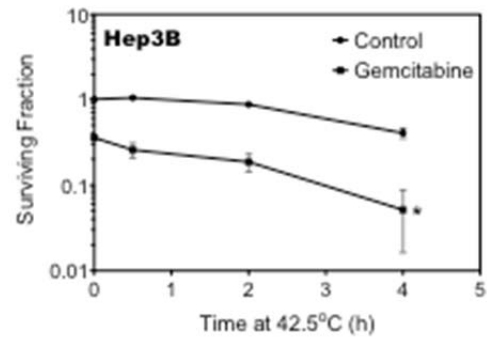
A. Experimental design



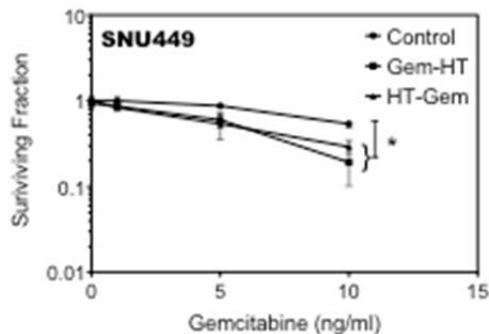
B



C



D



E

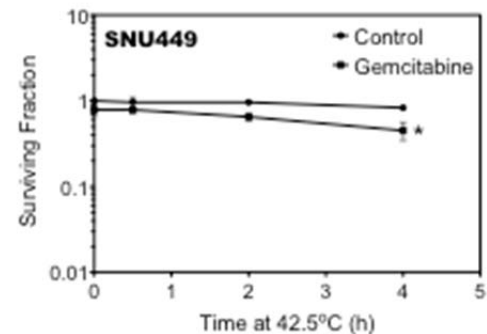


Figure 10. Hyperthermia sensitizes hepatocellular carcinoma cells to gemcitabine in a dose-dependent manner.

Panel A. Experimental scheme is presented

Panel B & D. Experimental design i, ii and iii were used.

Panel C & E. Experimental design iv was used.

*p < 0.05

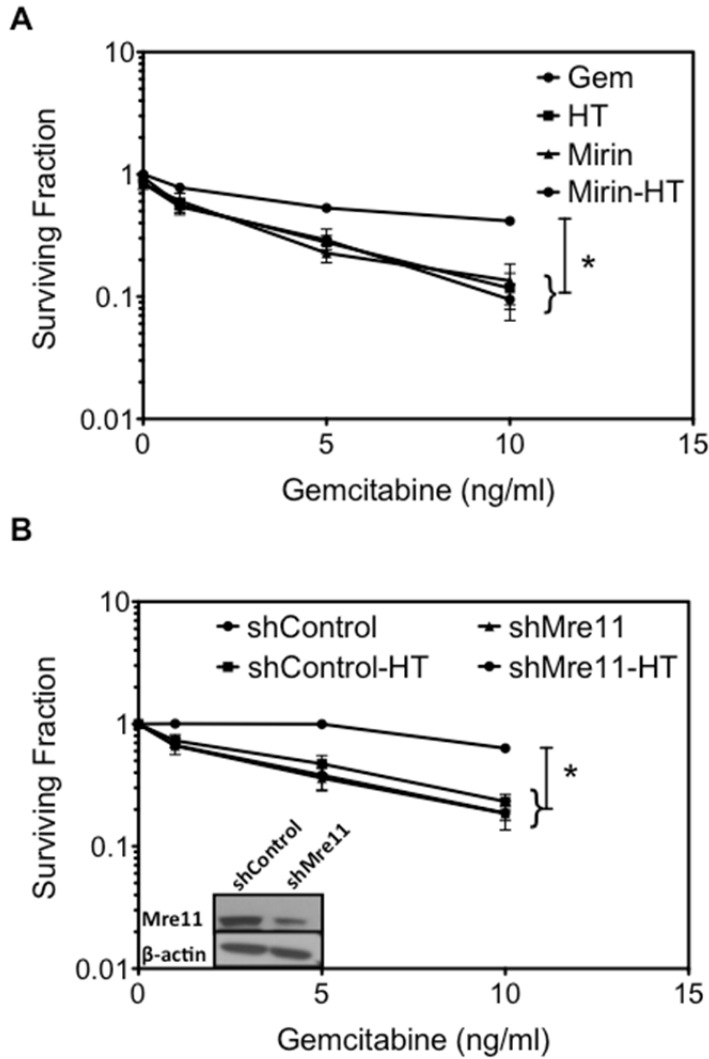


Figure 11. Hyperthermia-induced gemcitabine sensitivity of hepatocellular carcinoma cells is via a Mre11-dependent pathway

Panel A. Hep3B cells were treated with gemcitabine alone (Gem), hyperthermia +/- gemcitabine (HT), Mirin +/- gemcitabine (Mirin) or Hyperthermia and Mirin +/- gemcitabine (Mirin-HT). In all cases hyperthermia followed gemcitabine or mirin exposure. * $p < 0.05$

Panel B. Control (shControl) or Mre11 knockdown (shMre11) were treated with or without gemcitabine followed by +/- hyperthermia. * $p < 0.05$

3.5 Animal model studies

Two animal models of human primary hepatocellular carcinoma were developed using a wt-p53 HepG2 cell line or null-p53 Hep3B cell line in immune-deficient CB17 SCID mice. The cells were implanted in the liver to generate an orthotopic tumor model as detailed in the methods. We noted that both xenografts were locally aggressive, eroded (as opposed to invaded) the normal adjacent mouse liver and had no distant or intra-hepatic metastasis or extension in non-liver viscera. However, Hep3B xenografts were fast growing unlike the HepG2 xenografts. On histological analysis, both tumors appeared hyper-vascular with areas of spontaneous necrosis (Figure 12). We observed larger aberrant vessels with Hep3B xenografts, which were not seen with HepG2 xenografts. The xenograft models closely mimicked non-metastatic human primary hepatocellular carcinoma based on growth pattern, macroscopic and microscopic appearance.

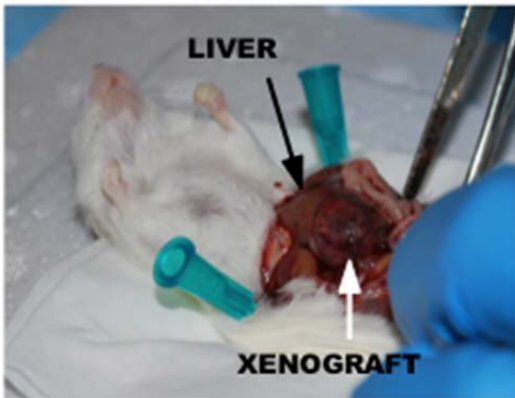
Figure 12. Animal model characterization (next page)

Panel A. A Hep3B xenograft is seen in the left lobe of CB17 SCID mouse liver at the time of necropsy.

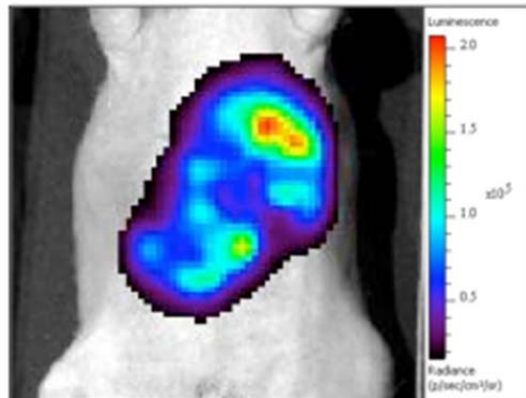
Panel B. The development of luciferase expressing Hep3B or HepG2 xenografts can be tracked using bioluminescence imaging.

Panel C-F. Histological analysis demonstrates that these xenografts mimic human hepatocellular carcinoma based on growth pattern, hyper-vascularity, erosion and spontaneous central necrosis.

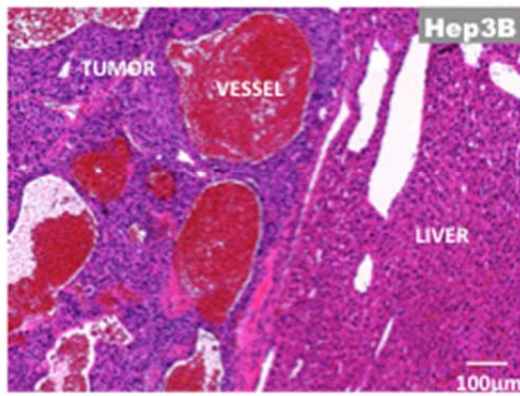
A



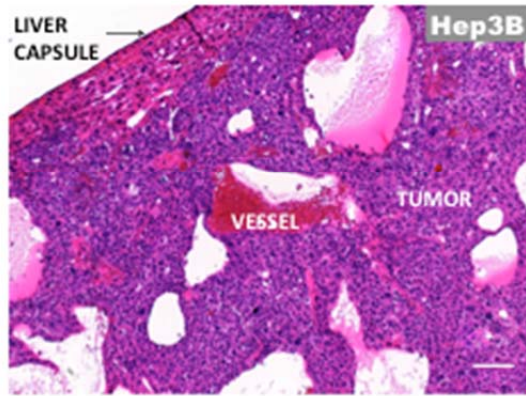
B



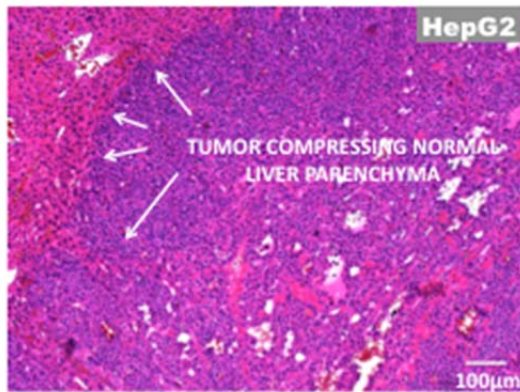
C



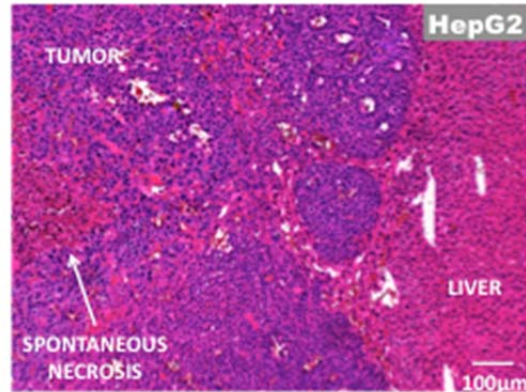
D



E



F



After establishing the tumor models, we evaluated if hyperthermia could be successfully delivered to the tumor tissue using the 13.56 MHz non-invasive Kanzius RF generator. For that purpose, we employed fiber-optic thermography to measure the temperature of liver tumor and normal liver in anesthetized mice subjected to RF field exposure for 10 min at 600W. Since fiberoptic thermography requires placement of a fiber-optic (400 micron diameter) probe under ultrasound guidance and is challenging for smaller tumors, we wanted to investigate if abdominal surface temperature as measured by infrared thermal imaging correlated with tumor temperature. This would allow us monitor thermal dose in real-time non-invasively for future experiments. The data are shown in figure 13.

After anesthesia and during placement of mice on the Rx head of the RF generator, we noted a drop in core body and surface temperature. For consistency we allowed the abdominal surface temperature to drop to 34°C before starting RF exposures. During a 10-minute RF exposure we observed a duration-dependent near-linear rise in Hep3B xenograft and normal liver temperature. Interestingly, normal livers heated significantly less than Hep3B xenografts, suggesting, some tumor selective heating effect of RF-field exposure. Abdominal surface temperatures recorded during these experiments demonstrated a strong linear correlation with tumor temperature ($R^2=0.99$). Prior reports have demonstrated that a 10-min RF exposure using the same parameters is safe with no detectable harm to normal tissues (86). Here we demonstrate that the same RF exposure can be used to deliver tumor selective hyperthermia to orthotopic liver tumors. However, the underlying reason for tumor selective hyperthermia is not evident from these

experiments. Thermal dose calculations as defined by cumulative equivalent minutes at 43°C (CEM43) were performed using the average time-temperature plots obtained from liver tumor and normal liver during a 10-minute RF exposure. We note that CEM43 for liver tumor was ~80 fold higher than that of normal liver (CEM43: 1401.6 vs. 17.5).

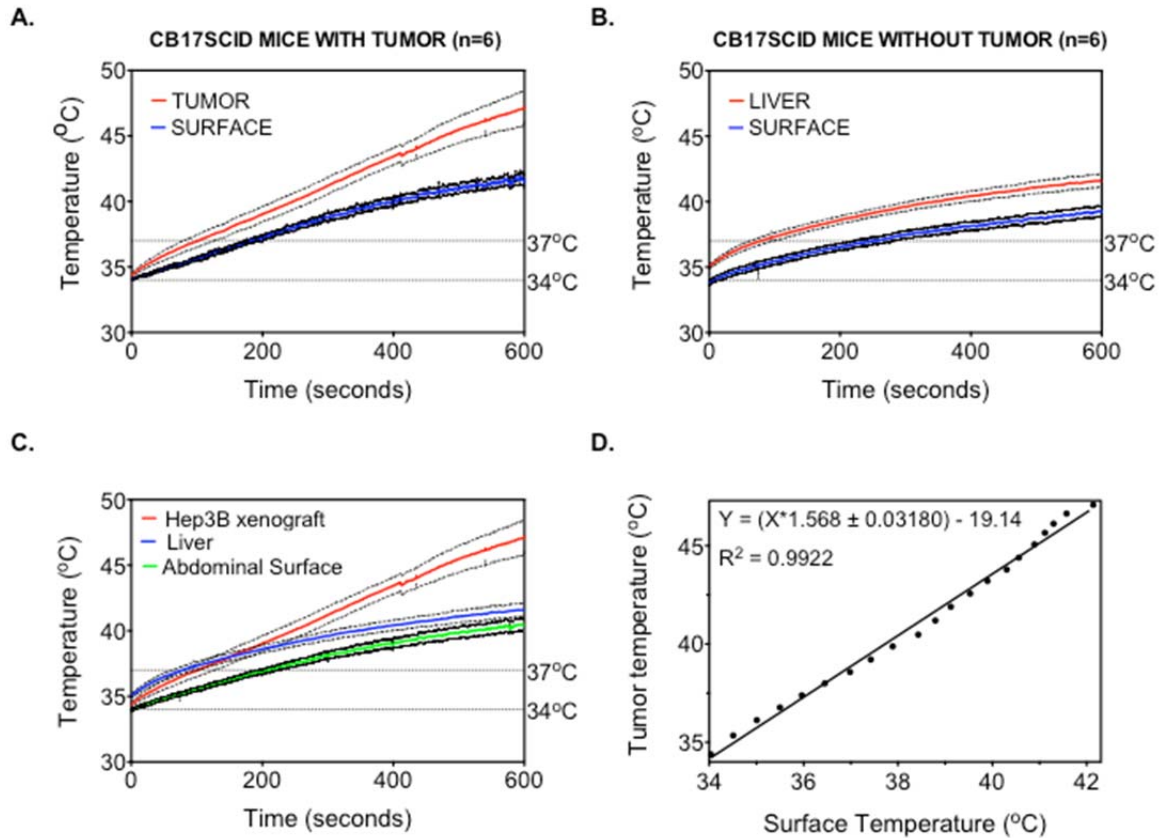


Figure 13. Thermal dose quantification in Hep3B xenografts under RF field exposure (13.56 MHz, 600W)

Panel A. Xenograft and abdominal surface temperatures were measured in real-time using fiber optic thermography and infrared thermography, respectively in tumor-bearing mice

Panel B. Similar measurements were performed on the normal livers of non-tumor-bearing mice.

Panel C. Data in Panel A and B are combined for comparative representation. Abdominal surface temperature is the composite average from tumored and non-tumor-bearing mice.

Panel D. Tumor and surface temperature from Panel A is plotted and was found to correlate in a linear fashion.

To determine the anti-tumor effect of hyperthermia alone or in combination with gemcitabine we used the same set-up as described above and in the Methods section. For the Hep3B orthotopic tumor model experiment, we allowed the tumors to grow for three weeks after implantation before starting treatment. At three week after implantation of cells, bioluminescence imaging was performed to confirm presence of tumors. Mice that developed tumors were randomized to one of five groups: Untreated, RF exposure alone, gemcitabine alone, gemcitabine followed 24 hours later by RF exposure, or RF exposure immediately followed by gemcitabine. This experimental design is comparable to *in vitro* studies reported above. The treatments were administered twice a week for 3 weeks for a total of 6 treatments. Gemcitabine dose administered was 70mg/kg/dose or 150mg/kg/week. This is approximately half the dose used in humans (1000mg/m²/week dose in a 1.7m human equals ~300mg/kg/week dose in a mouse). Twenty-four hours after the last treatment, mice were sacrificed and tumors were harvested, weighed and fixed in formalin for downstream analysis (Figure 14). At the end of the experiment, we noted that tumors in all treatment groups were significantly smaller and had a lower tumor mass than untreated controls ($p < 0.05$). On further analysis, we compared tumor mass of gemcitabine treated tumors with that of tumors that received combination therapy. We found that combination therapy was more effective than gemcitabine alone based on tumor mass ($p < 0.01$). Of note, there was no difference in tumor mass when comparing groups that received a different schedule of combination therapy. From these data we conclude that addition of hyperthermia

using the radiofrequency field enhances gemcitabine-mediated anti-tumor effect in Hep3B xenografts.

This experiment was repeated in the slow growing wt-p53 HepG2 xenograft model with some modifications in the design (Figure 15). Tumor presence was confirmed at 4 weeks instead of 3 weeks using bioluminescence imaging to allow the tumors to grow to a larger size. Mice with tumors were then randomized to one of five groups as detailed in the previous experiment. Treatments were performed once a week for a duration of 3 weeks instead of twice a week, keeping in mind the slow growing nature of these xenografts. Unlike Hep3B xenografts we found that HepG2 xenografts treated with RF exposure alone were not significantly different from untreated controls. However, gemcitabine-treated groups had significantly smaller tumors compared to mice treated with RF exposure alone or not treated. Similar to the Hep3B xenografts we found that addition of hyperthermia to gemcitabine significantly enhanced the anti-tumor effect of gemcitabine in HepG2 xenografts. Again, as with Hep3B xenografts no difference was noted between the two schedules of combination treatment tested.

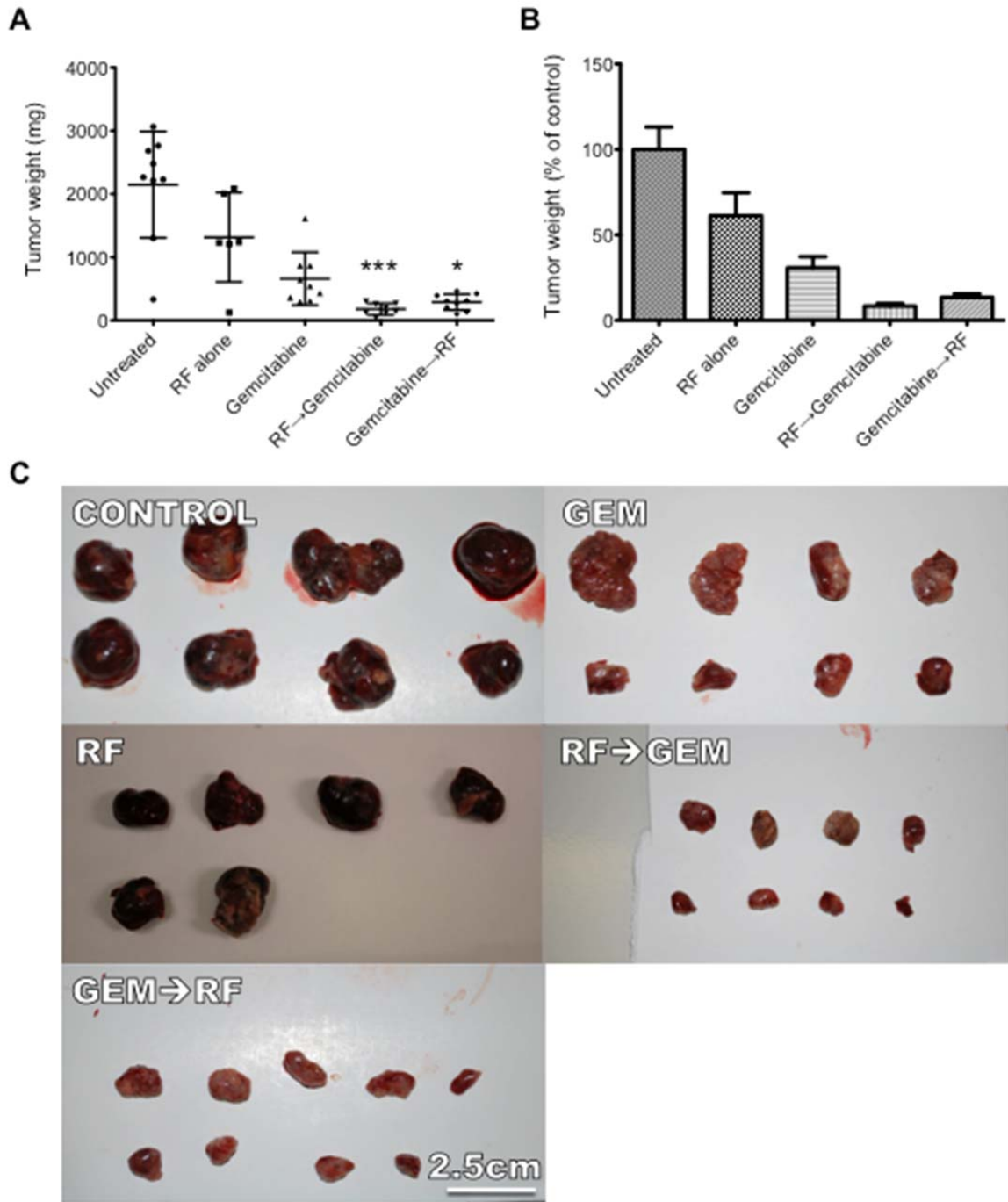


Figure 14. Efficacy of gemcitabine and RF combination therapy in mice bearing Hep3B xenografts

Tumor weight, percent growth inhibition and macroscopic appearance are represented in Panel A, B & C, respectively. (* $p < 0.05$, *** $p < 0.001$ vs. Gemcitabine)

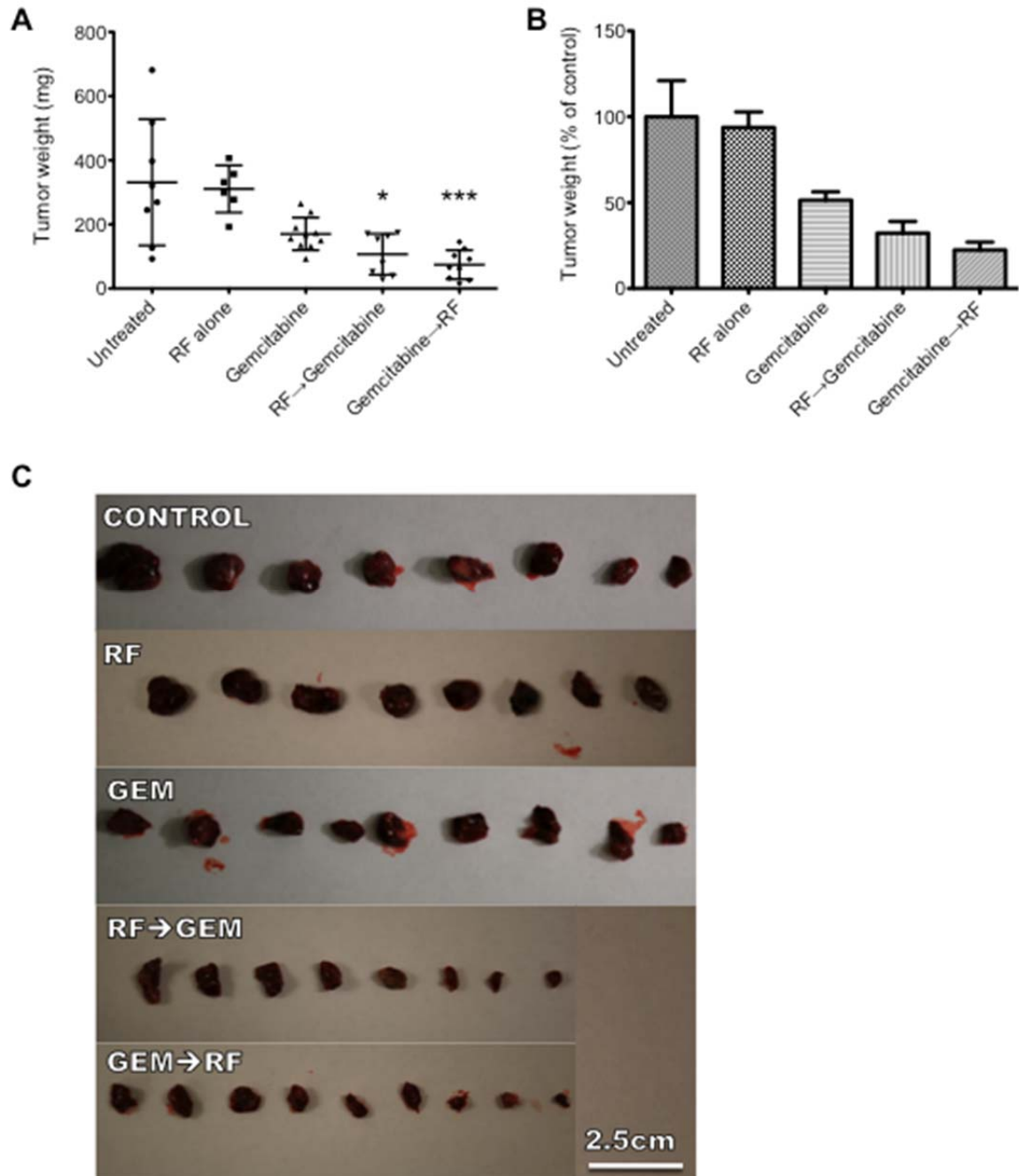


Figure 15. Efficacy of gemcitabine and RF combination therapy in mice bearing HepG2 xenografts

Tumor weight, percent growth inhibition and macroscopic appearance are represented in Panel A, B & C, respectively. (* $p < 0.05$, *** $p < 0.001$ vs. Gemcitabine)

From the *in vitro* studies we have established that Mre11 is a key thermolabile target that is important in the repair of gemcitabine-stalled replication forks. Inhibition of Mre11 exonuclease using mirin resulted in significant enhancement of gemcitabine cytotoxicity in the Hep3B cell line. Despite its weak inhibitory effects we wanted to evaluate if this thermomimetic response to mirin could be reproduced in an *in vivo* Hep3B xenograft model. For that purpose, 4 weeks after Hep3B cell implantation, mice bearing tumors were randomized to no treatment, gemcitabine alone (35mg/kg/dose), mirin alone (50mg/kg/dose) or a combination of gemcitabine and mirin. The treatment was repeated two times a week for two weeks. Of note, the dose of gemcitabine was reduced to half of that used in previous experiments to better demonstrate the synergistic interaction, if any. The dose of mirin chosen for this experiment was the maximum dose that could be dissolved in the maximum amount of DMSO that could be safely administered to the mice. All the mice not treated with mirin also received DMSO. The data shown in Figure 16 demonstrate that there were no statistically significant differences among the various tumor groups. We do note however, that the mice treated with the combination therapy had the lowest median tumor mass. Interestingly, we noted a bimodal distribution of tumor mass in the combination, which was not observed with other groups. The reason for this finding is not evident from this experiment, as we do not have correlative pharmacokinetic and pharmacodynamic data on mirin. With its weak inhibitory effects on Mre11, mirin is an unsuitable compound for drug development. We hope to repeat this experiment with more effective inhibitors of Mre11 in the future.

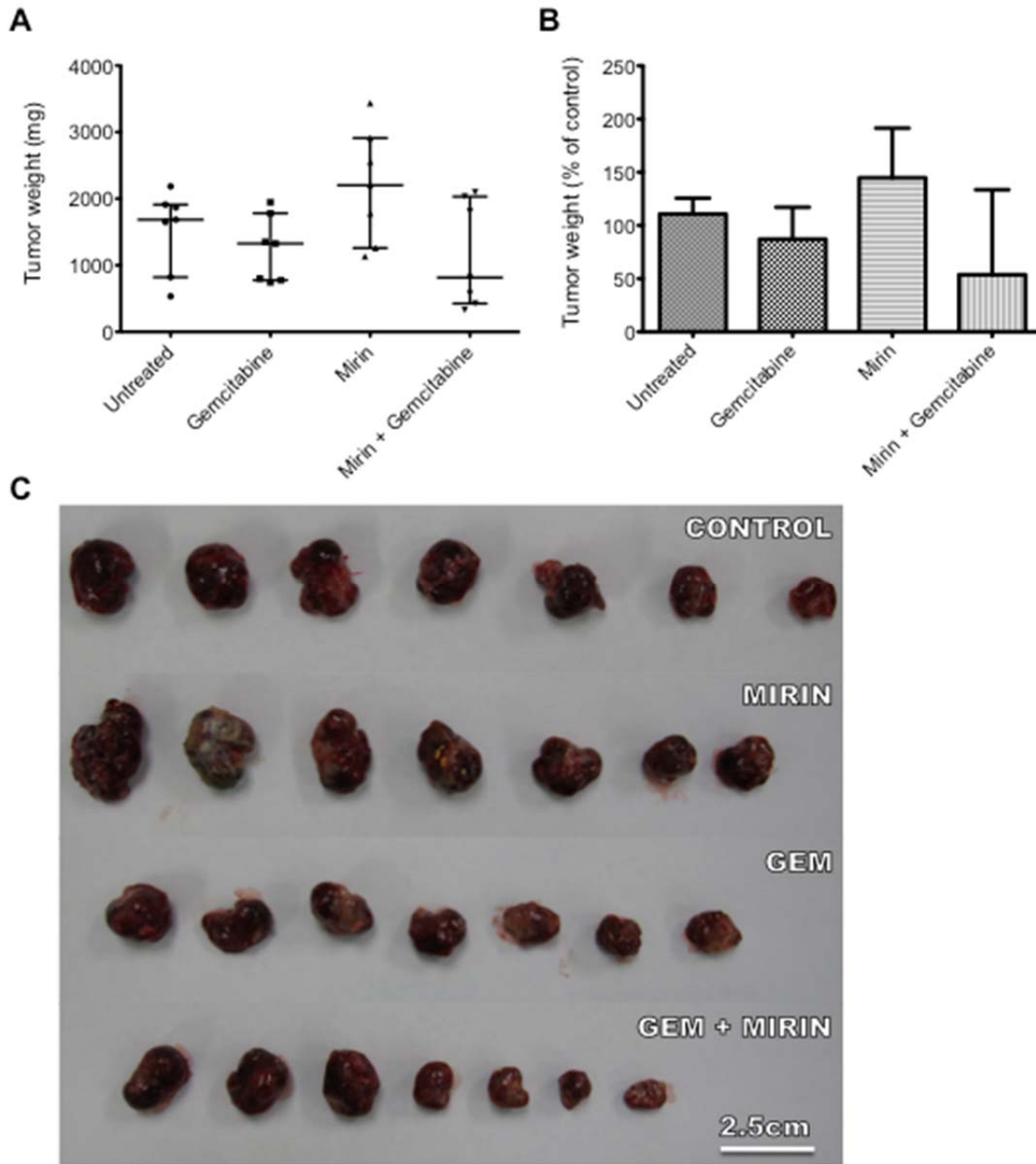


Figure 16. Efficacy of gemcitabine and Mirin combination therapy in mice bearing Hep3B xenografts

Tumor weight, percent growth inhibition and macroscopic appearance are represented in Panel A, B & C, respectively.

From these three animal experiments, we draw several important conclusions. First, RF exposure alone has an anti-tumor effect in Hep3B xenografts but not in HepG2 xenografts. Second, HepG2 xenografts are more sensitive to gemcitabine compared to Hep3B xenografts. Third, combination therapy with gemcitabine and RF hyperthermia was more effective than gemcitabine alone in both tumor models. Fourth, the schedule of combination therapy did not have an impact on anti-tumor efficacy for the two schedules tested in either tumor model. Finally, mirin, a water-insoluble, weak inhibitor of Mre11 exonuclease activity demonstrated some anti-tumor effect in combination with gemcitabine and no anti-tumor effect when used alone. However, better inhibitors and further investigation is needed to develop Mre11 inhibition as a thermomimetic approach to enhance gemcitabine toxicity.

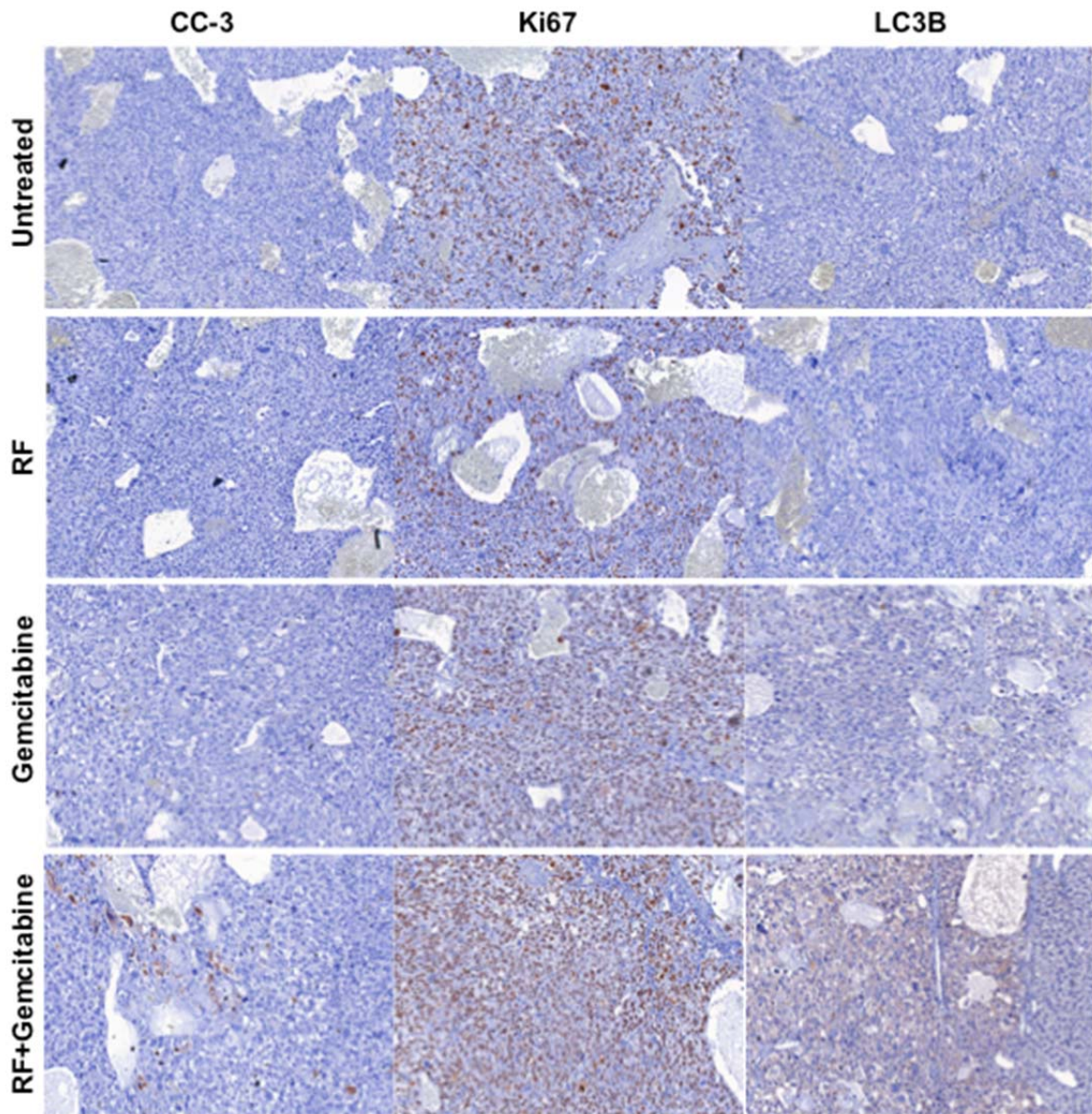
3.6 Histological analysis of human HCC xenografts from mice

Tumor tissues from the first Hep3B xenograft experiment were harvested 24 hours after the last treatment and analyzed. We evaluated the autophagy marker LC3B and apoptosis marker CC3-3 in various tumor tissues using colorimetric immunohistochemistry (Figure 17). Although tumors in the combination groups demonstrated more frequent CC-3 positive cells than tumors in other groups, the overall frequency of apoptotic cells was rare. Since Hep3B xenografts lack p53 expression, and apoptosis is tightly regulated by p53, this observation is not unexpected. We evaluated autophagy as a marker of cell death and noted that tumors that received combination treatment had a pronounced increase in

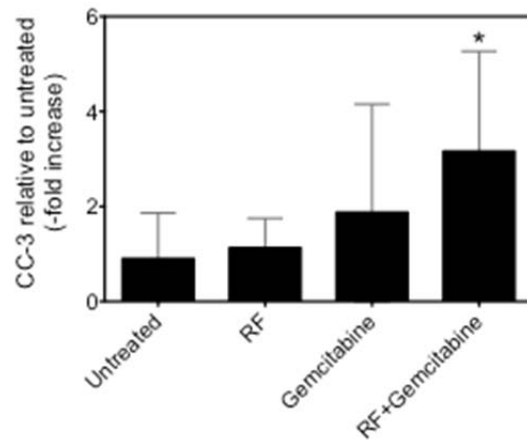
autophagy compared to tumors in other groups suggesting an important role in the observed anti-tumor effect. When evaluating proliferation using an S-phase specific marker, Ki67, we found an increase in staining. It seems contradictory to have increased proliferation in tumors with smaller mass. We interpret this to represent *in situ* synchronization of tumor cells in S-phase 24 hours after last dose of gemcitabine consistent with *in vitro* cell cycle analysis data.

Next we evaluated localization of the HRR-pathway proteins Mre11 and Rad51 to sites of stalled replication forks in tumors of mice in various groups. Stalled replication forks were detected by labeling γ -H2AX foci (Figure 18,19, 20). Consistent with *in vitro* data we observed decreased localization of the HRR-pathway proteins to sites of stalled replication forks. In addition we also noted a relatively higher proportion of γ -H2AX positive cells in tumors treated with the combination of gemcitabine and RF exposure in comparison with tumors in gemcitabine only group. We interpret this to represent the presence of persistently stalled replication forks or DNA damage in these tumors. Finally we also noted an increased aberrancy in the shape of nuclei in tumors treated with combination therapy compared to those treated with gemcitabine alone. These nuclei were irregular in shape and appeared fragmented suggestive of unrepaired DNA damage.

A.



B.



C.

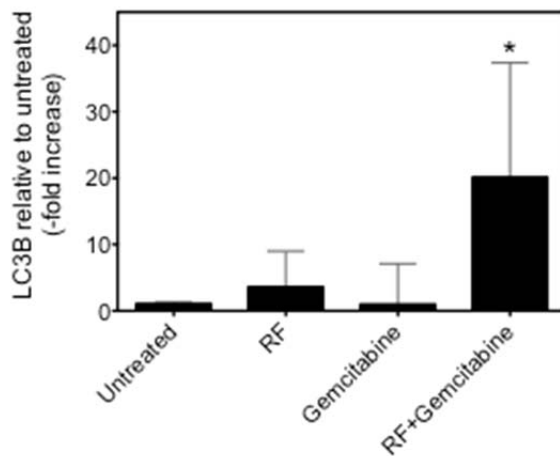


Figure 17. Immunohistochemical analysis for proliferation, apoptosis and autophagy

(A) Markers for apoptosis (CC-3), proliferation (Ki67) and autophagy (LC3B) were evaluated in Hep3B xenografts. Tumors treated with combination gemcitabine and RF therapy demonstrated increased apoptosis and autophagy compared to untreated, gemcitabine alone or RF alone controls. Increased proliferation (Ki67) in gemcitabine-treated tumor groups may represent *in situ* synchronization of cells in S-phase of the cell cycle. (B, C) Tumor tissue staining for CC-3 and LC3B was quantified and median (Inter-quartile range) is represented. * $p < 0.05$ Mann-Whitney Test (non-parametric)

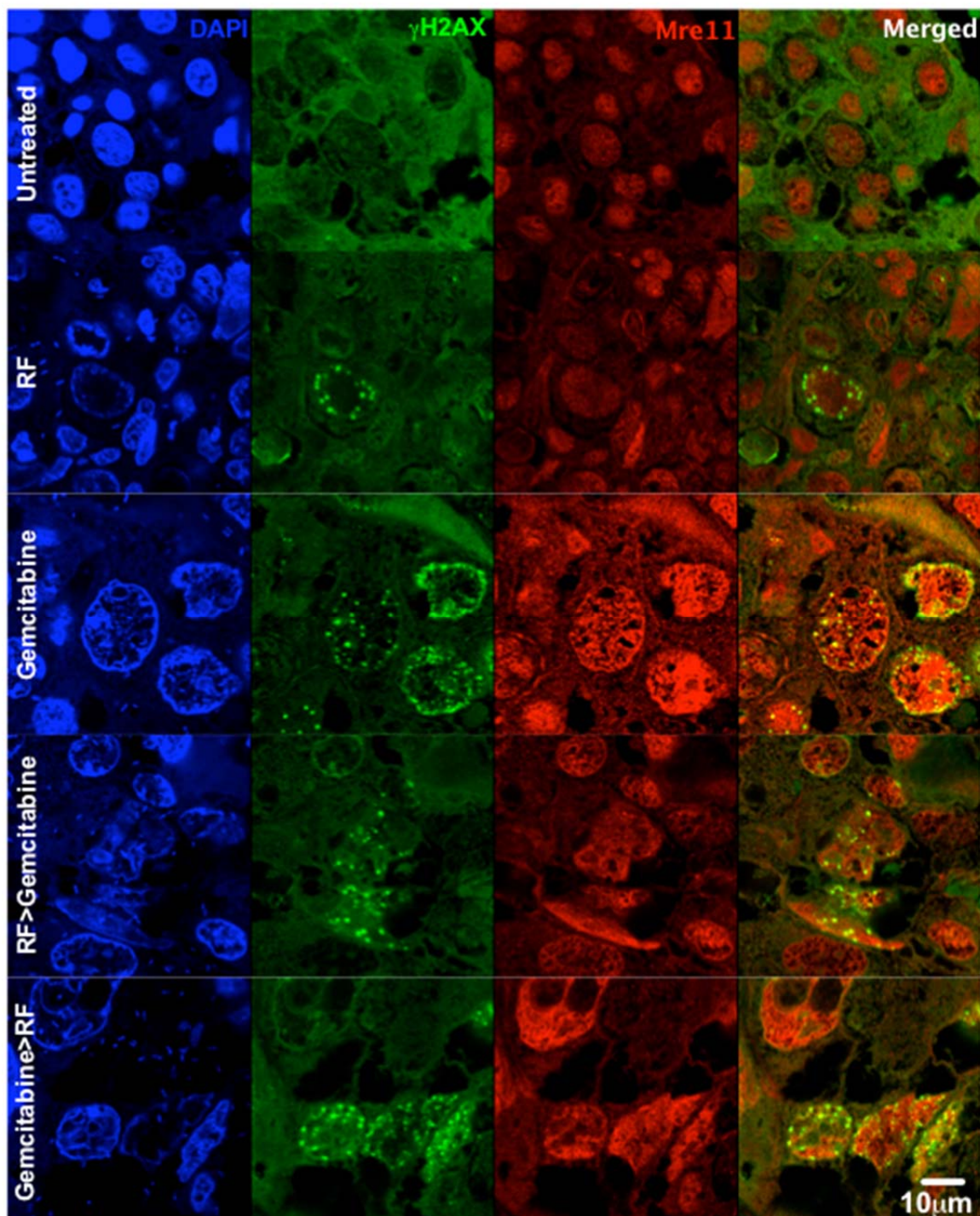


Figure 18. Inhibition of Mre11 localization to stalled forks *in vivo*

Hep3B xenografts were evaluated for colocalization of γ -H2AX and Mre11 foci. As shown RF exposure inhibits Mre11 localization to stalled replication forks.

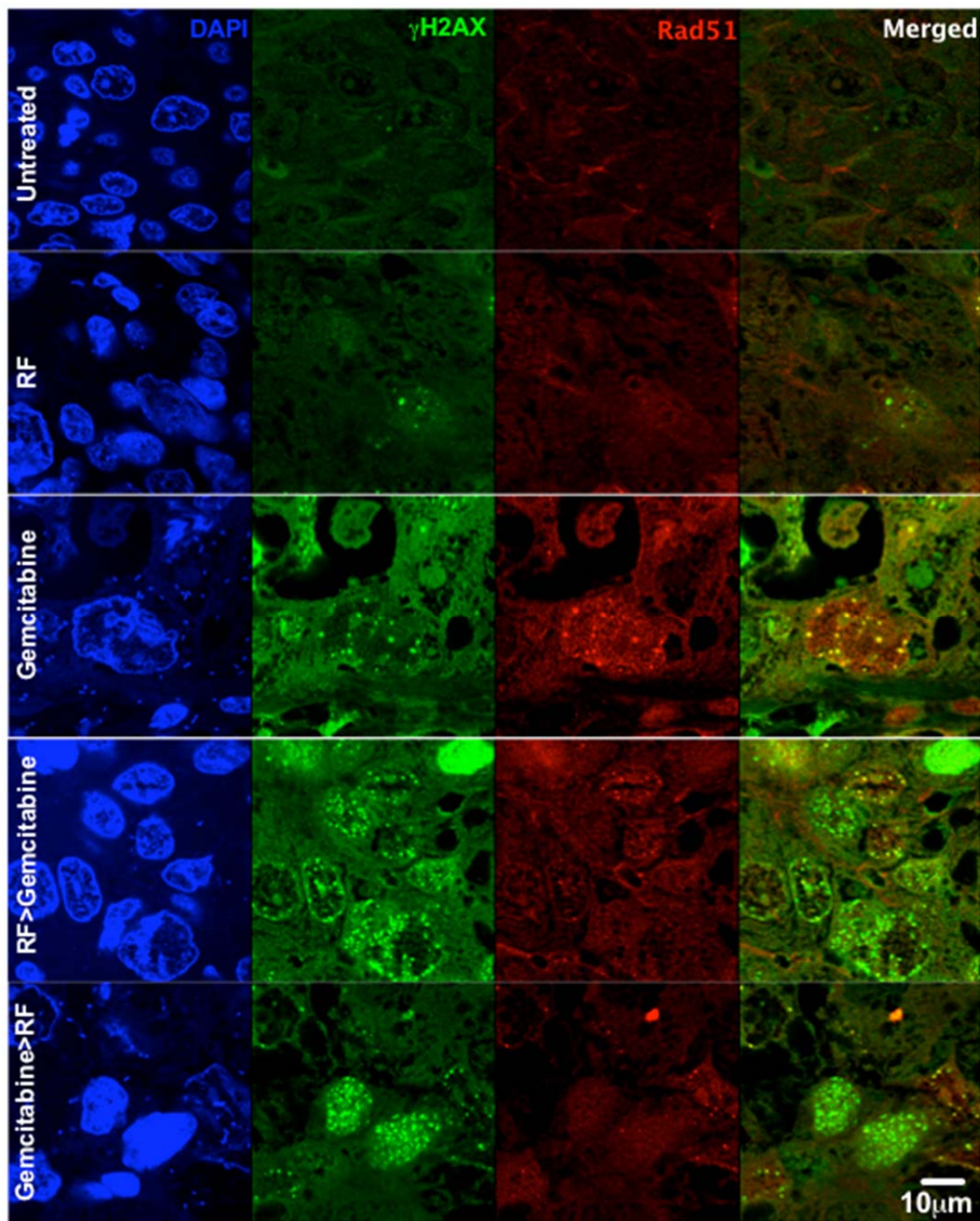
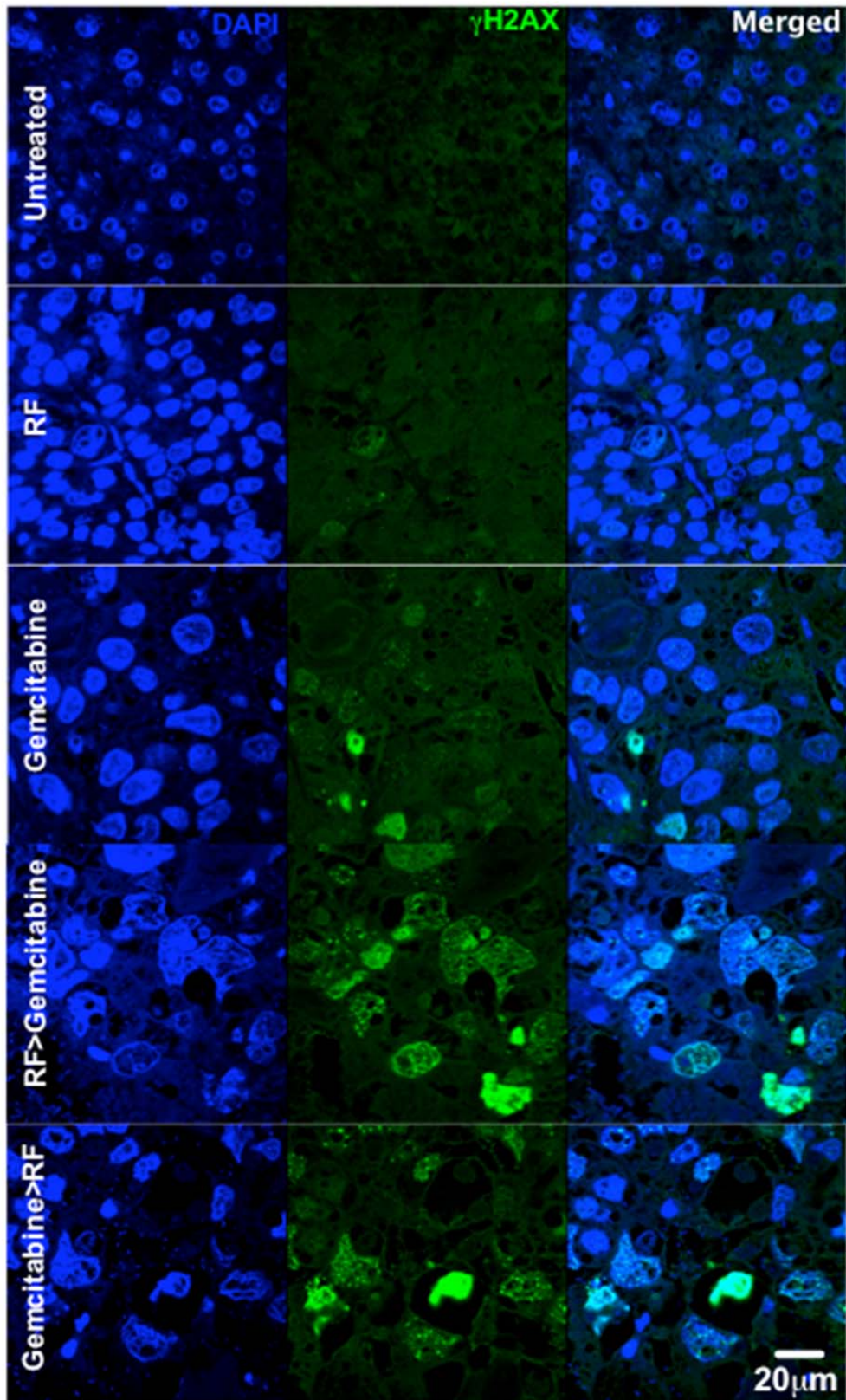


Figure 19. Inhibition of Rad51 localization to stalled forks *in vivo*

Hep3B xenografts were evaluated for colocalization of γ -H2AX and Rad51 foci. As shown RF exposure inhibits Rad51 localization to stalled replication forks.

A



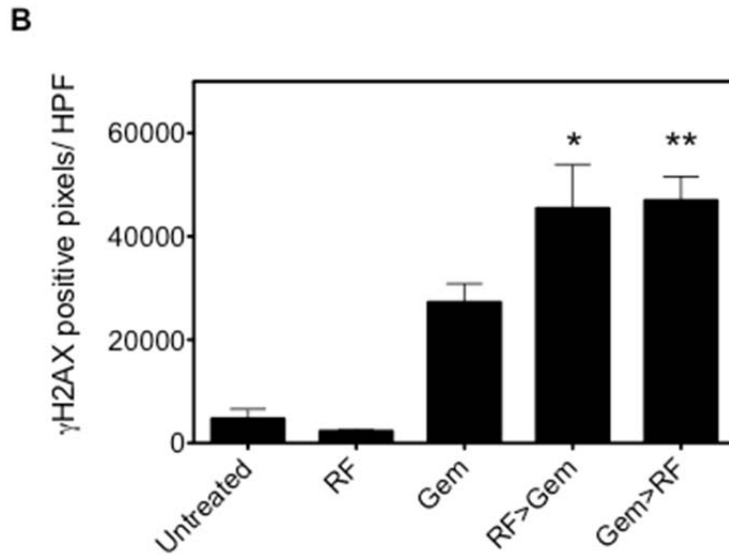


Figure 20. RF exposure inhibits resolution of gemcitabine-induced DNA damage in Hep3B xenografts

Panel A. Sites of DNA damage were evaluated using fluorescence immunohistochemistry for γ -H2AX. Also note the increased nuclear fragmentation in the DAPI channel for combination therapy groups.

Panel B. Tumors treated with combination therapy demonstrate significantly higher γ -H2AX staining. * $p < 0.05$, ** $p < 0.01$ vs. gemcitabine.

4. DISCUSSION

Several findings of this study have important implications for rational drug combinations and multi-modality treatment of hepatocellular carcinoma. First, we demonstrate that the HRR-pathway is invaluable in the repair of gemcitabine-stalled replication forks. Second, the synergy between gemcitabine and hyperthermia has been previously reported. However, a mechanistic understanding has been lacking and the data presented here provide a rational explanation for this synergy. Third, we demonstrate that the relevant thermal dose necessary for such synergistic interaction can be achieved in pre-clinical mouse models using a non-invasive radiofrequency field generator in a tumor selective fashion. Finally, these data provide an initial platform for further development of thermomimetic approaches to circumvent gemcitabine chemoresistance in hepatocellular carcinoma. These findings are discussed in more detail below.

Gemcitabine is the only nucleoside analogue with a potent activity in solid tumors. Its unique self-potentiating mechanism (discussed in the introduction) is thought to be important for this activity. Several pathways have been implicated in chemoresistance of solid tumors to gemcitabine. However most of these involve reduced conversion of pro-drug (gemcitabine) to active drug (gemcitabine triphosphate) leading to decreased incorporation of gemcitabine in the DNA. Our data demonstrate that clinically achievable intracellular concentration (1 μM) was sufficient to arrest cell cycle in hepatocellular carcinoma cells suggesting adequate incorporation of gemcitabine in the DNA. Moreover, 24 hours after removal of gemcitabine, these cells resumed their cell cycle. Therefore pathways to repair

gemcitabine-stalled replication forks must exist and may contribute to drug resistance.

We evaluated proteins of the HRR-pathway believed to be important in the restart of hydroxyurea-stalled replication forks. We failed to demonstrate PAR localization to these sites as observed by Bryant *et al.* when evaluating hydroxyurea-stalled replication forks (66). We attribute this discrepancy to our inability to detect PAR foci due to high baseline levels of PAR residues in the nuclei of cancer cells. It may also reflect differences in the replication poison used (gemcitabine vs. hydroxyurea) or differences in the cell lines investigated. However, we find that RPA, Mre11 and Rad51 readily accumulate at sites of stalled replication forks. These findings are consistent with prior reports (62, 66, 93). We find that Mre11 knockdown cells or cells where mre11 exonuclease activity was inhibited by mirin were more sensitive to gemcitabine than control cells demonstrating the significance of this HRR-pathway protein in gemcitabine resistance. This result is consistent with observations of Ewald *et al.* with their study on leukemia cell lines (62).

After demonstrating HRR-pathway as a survival mechanism for cancer cells treated with gemcitabine, we asked if the same mechanism may be involved in anti-tumor synergy of gemcitabine and hyperthermia. When evaluating HRR protein levels after hyperthermia we noted that mild-moderate hyperthermia had a transient effect on PARP1 levels. Similarly levels of Nbs1, Rad50, Rad51 and p53 were minimally affected. We note partial degradation of BRCA2 in one cell line. However partial degradation of Mre11 was consistently observed in all cell lines.

Thermolability of Mre11 has been recently reported in a study where only 10 min at 42.5°C reduced Mre11 exonuclease function to 10% of untreated control (81). On further analysis we found that Mre11 and downstream Rad51 failed to localize at gemcitabine-stalled replication forks in cells pretreated with mild hyperthermia. Assimilating these observations and those from Dynlacht *et al.* we attribute this effect to thermal denaturation of Mre11.

We demonstrate that hyperthermia has no effect on emergence from G1/S arrest in cells with gemcitabine-stalled replication forks. In fact these cells progressed through early and mid-S phase without much delay. However, we noted a prolonged passage through late S and G2 phase, which is characteristic for cells deficient in post-replication recombination repair (94). When evaluating synergy of gemcitabine and hyperthermia Vertees *et al.* noted a similar enhancement of cells arrested in G2/M phase with combination therapy (89). This delay in recovery was also observed with persistent γ H2AX staining in our study. Ultimately, we find that this inhibition of the Mre11-dependent HRR pathway by hyperthermia is responsible for decreased clonogenic survival and cell death.

It is important to discuss thermal degradation of BRCA2 and its effects on HRR of stalled replication forks because BRCA2 plays two essential roles at the stalled replication forks. BRCA2 prevents excessive nucleolytic degradation of stalled forks by Mre11, an effect associated with genomic instability (82). Therefore, degradation of BRCA2 is expected to increase excision of gemcitabine by Mre11 and contribute to chemoresistance. Conversely, BRCA2 participates in Rad51 loading in HRR pathway (95). In this case, degradation of BRCA2 is expected to

inhibit repair of gemcitabine-stalled replication forks and have the opposite effect. Because of this paradoxical effect at stalled replication forks it is unlikely that BRCA2 is responsible for thermal enhancement of gemcitabine toxicity as observed here. These findings also imply that synergistic interaction between hyperthermia and gemcitabine will ultimately depend on the relative effect on heat on BRCA2 compared to that on Mre11. For instance, thermal degradation of BRCA2 without Mre11 inhibition may not only contribute to gemcitabine resistance but also genomic instability as detailed in a report by Schlacher *et al.* (82). Conversely, tumors already deficient in BRCA2 may be more susceptible to thermal sensitization of gemcitabine therapy. This speculation is supported by findings of Ying *et al.* who demonstrate BRCA2 deficient cells to be more susceptible to Mre11 inhibition (93). These speculations however, need to be tested in future studies.

We deduce from the mechanism of action described in this study that inhibition of HRR by hyperthermia will be most effective when cells recovering from gemcitabine are passing through late S and G2 phase of the cell cycle. This underscores the need to optimize the dosing schedule in future studies. From animal experiments we find that the schedule where the two therapies were given in quick succession was comparable to the schedule where hyperthermia was given 24 hours after gemcitabine. We explain these findings based on the duration of the effect of hyperthermia on HRR that lasts 39-48 hours. Our study also helps explain findings of Van Bree *et al.* who noted maximum synergistic effect 24-48 hours after gemcitabine dose in a rhabdomyosarcoma model (90). Even though comparative

cell cycle analysis was not provided in that study, we expect the cells to be in late S or G2 phase 24-48 hours after gemcitabine dose based on our findings.

While our data suggest that passage of cells through late S/ G2 phase with stalled replication forks increases tumor cell kill, the mechanism remains to be elucidated. Vertees *et al.* reported apoptosis to be a significant mechanism from this combination therapy (89). In our study we noted that apoptosis was increased in tumors treated with combination therapy however, the occurrence of apoptosis was infrequent. This may be due to the lack of p53 in our Hep3B tumor model. In support of alternative mechanisms we noted increased nuclear fragmentation and increased autophagy in tumors treated with combination therapy compared to controls.

5. Conclusion and future studies

From the findings of this study we conclude that the HRR pathway is important in the repair of gemcitabine-stalled replication forks. Inhibition of the HRR-pathway protein, Mre11, enhances the toxicity of gemcitabine in cancer cells *in vitro* and *in vivo*. Thermal enhancement of anti-tumor effect of gemcitabine is mediated through inhibition of Mre11-dependent HRR pathway by denaturation and degradation of Mre11. Non-invasive RF field-induced tumor selective hyperthermia in combination with gemcitabine is superior to either modality alone in orthotopic mouse models of hepatocellular carcinoma.

Future studies already underway will build on these findings to develop a non-invasive combined modality treatment for patients with hepatocellular carcinoma. For translation of this modality to clinic, certain questions need to be answered first. Specifically, our data strongly suggest Mre11 as a key enzyme responsible for the excision of gemcitabine from stalled replication forks. To confirm this hypothesis, exonuclease assays will be performed using purified Mre11. In addition the effect of hyperthermia on the ability of Mre11 to excise gemcitabine will also be investigated. Our data demonstrate that the effect of hyperthermia is cell cycle phase-dependent with maximum effect in the late S and G2 phase. Further studies will utilize this information to optimize temporal parameters for maximum anti-tumor effects. The findings of the study indicate that the currently available inhibitor of Mre11 is not suitable for clinical use. More potent inhibitors need to be developed for a thermo-mimetic approach to cancer therapy. In addition, the effects of hyperthermia on Mre11 can be further exploited by combination with other DNA

damaging agents that activate the HRR-pathway such as other replication inhibitors e.g. hydroxyurea, nucleoside analogues or double-strand break inducers including platinum compounds, alkylating agents and topoisomerase inhibitors. Finally, translation of this modality to the clinic will also require parallel development of the non-invasive RF generator hyperthermia system. We are currently performing large animal studies to evaluate the safety and efficacy of this system before use in humans.

Bibliography

1. Altekruse, S. F., K. A. McGlynn, L. A. Dickie, and D. E. Kleiner. Hepatocellular carcinoma confirmation, treatment, and survival in surveillance, epidemiology, and end results registries, 1992-2008. *Hepatology* 55:476-482.
2. Jemal, A., F. Bray, M. M. Center, J. Ferlay, E. Ward, and D. Forman. Global cancer statistics. *CA Cancer J Clin* 61:69-90.
3. Perz, J. F., G. L. Armstrong, L. A. Farrington, Y. J. Hutin, and B. P. Bell. 2006. The contributions of hepatitis B virus and hepatitis C virus infections to cirrhosis and primary liver cancer worldwide. *J Hepatol* 45:529-538.
4. El-Serag, H. B., J. A. Davila, N. J. Petersen, and K. A. McGlynn. 2003. The continuing increase in the incidence of hepatocellular carcinoma in the United States: an update. *Ann Intern Med* 139:817-823.
5. Davila, J. A., R. O. Morgan, Y. Shaib, K. A. McGlynn, and H. B. El-Serag. 2004. Hepatitis C infection and the increasing incidence of hepatocellular carcinoma: a population-based study. *Gastroenterology* 127:1372-1380.
6. Prates, M. D., and F. O. Torres. 1965. A cancer survey in Lourenco Marques, Portuguese East Africa. *J Natl Cancer Inst* 35:729-757.
7. Sherman, M., K. M. Peltekian, and C. Lee. 1995. Screening for hepatocellular carcinoma in chronic carriers of hepatitis B virus: incidence and prevalence of hepatocellular carcinoma in a North American urban population. *Hepatology* 22:432-438.

8. Bugianesi, E., N. Leone, E. Vanni, G. Marchesini, F. Brunello, P. Carucci, A. Musso, P. De Paolis, L. Capussotti, M. Salizzoni, and M. Rizzetto. 2002. Expanding the natural history of nonalcoholic steatohepatitis: from cryptogenic cirrhosis to hepatocellular carcinoma. *Gastroenterology* 123:134-140.
9. Bressac, B., M. Kew, J. Wands, and M. Ozturk. 1991. Selective G to T mutations of p53 gene in hepatocellular carcinoma from southern Africa. *Nature* 350:429-431.
10. Tsai, J. F., J. E. Jeng, L. Y. Chuang, M. S. Ho, Y. C. Ko, Z. Y. Lin, M. Y. Hsieh, S. C. Chen, W. L. Chuang, L. Y. Wang, M. L. Yu, and C. Y. Dai. 2004. Habitual betel quid chewing and risk for hepatocellular carcinoma complicating cirrhosis. *Medicine (Baltimore)* 83:176-187.
11. Ueno, Y., S. Nagata, T. Tsutsumi, A. Hasegawa, M. F. Watanabe, H. D. Park, G. C. Chen, G. Chen, and S. Z. Yu. 1996. Detection of microcystins, a blue-green algal hepatotoxin, in drinking water sampled in Haimen and Fusui, endemic areas of primary liver cancer in China, by highly sensitive immunoassay. *Carcinogenesis* 17:1317-1321.
12. Freedman, N. D., A. J. Cross, K. A. McGlynn, C. C. Abnet, Y. Park, A. R. Hollenbeck, A. Schatzkin, J. E. Everhart, and R. Sinha. Association of meat and fat intake with liver disease and hepatocellular carcinoma in the NIH-AARP cohort. *J Natl Cancer Inst* 102:1354-1365.
13. Yang, W. S., P. Va, F. Bray, S. Gao, J. Gao, H. L. Li, and Y. B. Xiang. The role of pre-existing diabetes mellitus on hepatocellular carcinoma occurrence

- and prognosis: a meta-analysis of prospective cohort studies. *PLoS One* 6:e27326.
14. Welzel, T. M., B. I. Graubard, S. Zeuzem, H. B. El-Serag, J. A. Davila, and K. A. McGlynn. Metabolic syndrome increases the risk of primary liver cancer in the United States: a study in the SEER-Medicare database. *Hepatology* 54:463-471.
 15. Kew, M. C., H. A. Dos Santos, and S. Sherlock. 1971. Diagnosis of primary cancer of the liver. *Br Med J* 4:408-411.
 16. 1998. A new prognostic system for hepatocellular carcinoma: a retrospective study of 435 patients: the Cancer of the Liver Italian Program (CLIP) investigators. *Hepatology* 28:751-755.
 17. Vauthey, J. N., D. Klimstra, D. Franceschi, Y. Tao, J. Fortner, L. Blumgart, and M. Brennan. 1995. Factors affecting long-term outcome after hepatic resection for hepatocellular carcinoma. *Am J Surg* 169:28-34; discussion 34-25.
 18. Yao, F. Y., L. Ferrell, N. M. Bass, P. Bacchetti, N. L. Ascher, and J. P. Roberts. 2002. Liver transplantation for hepatocellular carcinoma: comparison of the proposed UCSF criteria with the Milan criteria and the Pittsburgh modified TNM criteria. *Liver Transpl* 8:765-774.
 19. Llovet, J. M., A. M. Di Bisceglie, J. Bruix, B. S. Kramer, R. Lencioni, A. X. Zhu, M. Sherman, M. Schwartz, M. Lotze, J. Talwalkar, and G. J. Gores. 2008. Design and endpoints of clinical trials in hepatocellular carcinoma. *J Natl Cancer Inst* 100:698-711.

20. Bharat, A., D. B. Brown, J. S. Crippin, J. E. Gould, J. A. Lowell, S. Shenoy, N. M. Desai, and W. C. Chapman. 2006. Pre-liver transplantation locoregional adjuvant therapy for hepatocellular carcinoma as a strategy to improve longterm survival. *J Am Coll Surg* 203:411-420.
21. Bruix, J., and J. M. Llovet. 2002. Prognostic prediction and treatment strategy in hepatocellular carcinoma. *Hepatology* 35:519-524.
22. Soini, Y., N. Virkajarvi, H. Raunio, and P. Paakko. 1996. Expression of P-glycoprotein in hepatocellular carcinoma: a potential marker of prognosis. *J Clin Pathol* 49:470-473.
23. Huang, C. C., M. C. Wu, G. W. Xu, D. Z. Li, H. Cheng, Z. X. Tu, H. Q. Jiang, and J. R. Gu. 1992. Overexpression of the MDR1 gene and P-glycoprotein in human hepatocellular carcinoma. *J Natl Cancer Inst* 84:262-264.
24. Caruso, M. L., and A. M. Valentini. 1999. Overexpression of p53 in a large series of patients with hepatocellular carcinoma: a clinicopathological correlation. *Anticancer Res* 19:3853-3856.
25. Llovet, J. M., S. Ricci, V. Mazzaferro, P. Hilgard, E. Gane, J. F. Blanc, A. C. de Oliveira, A. Santoro, J. L. Raoul, A. Forner, M. Schwartz, C. Porta, S. Zeuzem, L. Bolondi, T. F. Greten, P. R. Galle, J. F. Seitz, I. Borbath, D. Haussinger, T. Giannaris, M. Shan, M. Moscovici, D. Voliotis, and J. Bruix. 2008. Sorafenib in advanced hepatocellular carcinoma. *N Engl J Med* 359:378-390.

26. Yang, T. S., Y. C. Lin, J. S. Chen, H. M. Wang, and C. H. Wang. 2000. Phase II study of gemcitabine in patients with advanced hepatocellular carcinoma. *Cancer* 89:750-756.
27. Kubicka, S., K. L. Rudolph, M. K. Tietze, M. Lorenz, and M. Manns. 2001. Phase II study of systemic gemcitabine chemotherapy for advanced unresectable hepatobiliary carcinomas. *Hepatogastroenterology* 48:783-789.
28. Ulrich-Pur, H., G. V. Kornek, W. Fiebiger, B. Schull, M. Raderer, and W. Scheithauer. 2001. Treatment of advanced hepatocellular carcinoma with biweekly high-dose gemcitabine. *Oncology* 60:313-315.
29. Fuchs, C. S., J. W. Clark, D. P. Ryan, M. H. Kulke, H. Kim, C. C. Earle, M. Vincitore, R. J. Mayer, and K. E. Stuart. 2002. A phase II trial of gemcitabine in patients with advanced hepatocellular carcinoma. *Cancer* 94:3186-3191.
30. Tempero, M., W. Plunkett, V. Ruiz Van Haperen, J. Hainsworth, H. Hochster, R. Lenzi, and J. Abbruzzese. 2003. Randomized phase II comparison of dose-intense gemcitabine: thirty-minute infusion and fixed dose rate infusion in patients with pancreatic adenocarcinoma. *J Clin Oncol* 21:3402-3408.
31. Guan, Z., Y. Wang, S. Maoleekoonpaioj, Z. Chen, W. S. Kim, V. Ratanatharathorn, W. H. Reece, T. W. Kim, and M. Lehnert. 2003. Prospective randomised phase II study of gemcitabine at standard or fixed dose rate schedule in unresectable hepatocellular carcinoma. *Br J Cancer* 89:1865-1869.
32. Louafi, S., V. Boige, M. Ducreux, L. Bonyhay, T. Mansourbakht, T. de Baere, A. Asnacios, L. Hannoun, T. Poynard, and J. Taieb. 2007. Gemcitabine plus

- oxaliplatin (GEMOX) in patients with advanced hepatocellular carcinoma (HCC): results of a phase II study. *Cancer* 109:1384-1390.
33. Parikh, P. M., J. Fuloria, G. Babu, D. C. Doval, B. S. Awasthy, V. R. Pai, P. S. Prabhakaran, and A. B. Benson. 2005. A phase II study of gemcitabine and cisplatin in patients with advanced hepatocellular carcinoma. *Trop Gastroenterol* 26:115-118.
 34. Zhu, A. X., L. S. Blaszowsky, D. P. Ryan, J. W. Clark, A. Muzikansky, K. Horgan, S. Sheehan, K. E. Hale, P. C. Enzinger, P. Bhargava, and K. Stuart. 2006. Phase II study of gemcitabine and oxaliplatin in combination with bevacizumab in patients with advanced hepatocellular carcinoma. *J Clin Oncol* 24:1898-1903.
 35. Yang, T. S., C. H. Wang, R. K. Hsieh, J. S. Chen, and M. C. Fung. 2002. Gemcitabine and doxorubicin for the treatment of patients with advanced hepatocellular carcinoma: a phase I-II trial. *Ann Oncol* 13:1771-1778.
 36. Mackey, J. R., R. S. Mani, M. Selner, D. Mowles, J. D. Young, J. A. Belt, C. R. Crawford, and C. E. Cass. 1998. Functional nucleoside transporters are required for gemcitabine influx and manifestation of toxicity in cancer cell lines. *Cancer Res* 58:4349-4357.
 37. Achiwa, H., T. Oguri, S. Sato, H. Maeda, T. Niimi, and R. Ueda. 2004. Determinants of sensitivity and resistance to gemcitabine: the roles of human equilibrative nucleoside transporter 1 and deoxycytidine kinase in non-small cell lung cancer. *Cancer Sci* 95:753-757.

38. Schy, W. E., L. W. Hertel, J. S. Kroin, L. B. Bloom, M. F. Goodman, and F. C. Richardson. 1993. Effect of a template-located 2',2'-difluorodeoxycytidine on the kinetics and fidelity of base insertion by Klenow (3'-->5'exonuclease-) fragment. *Cancer Res* 53:4582-4587.
39. Heinemann, V., Y. Z. Xu, S. Chubb, A. Sen, L. W. Hertel, G. B. Grindey, and W. Plunkett. 1992. Cellular elimination of 2',2'-difluorodeoxycytidine 5'-triphosphate: a mechanism of self-potential. *Cancer Res* 52:533-539.
40. Heinemann, V., Y. Z. Xu, S. Chubb, A. Sen, L. W. Hertel, G. B. Grindey, and W. Plunkett. 1990. Inhibition of ribonucleotide reduction in CCRF-CEM cells by 2',2'-difluorodeoxycytidine. *Mol Pharmacol* 38:567-572.
41. Bengala, C., V. Guarneri, E. Giovannetti, M. Lencioni, E. Fontana, V. Mey, A. Fontana, U. Boggi, M. Del Chiaro, R. Danesi, S. Ricci, F. Mosca, M. Del Tacca, and P. F. Conte. 2005. Prolonged fixed dose rate infusion of gemcitabine with autologous haemopoietic support in advanced pancreatic adenocarcinoma. *Br J Cancer* 93:35-40.
42. Dumontet, C., K. Fabianowska-Majewska, D. Mantincic, E. Callet Bauchu, I. Tigaud, V. Gandhi, M. Lepoivre, G. J. Peters, M. O. Rolland, D. Wyczechowska, X. Fang, S. Gazzo, D. A. Voorn, A. Vanier-Viorner, and J. MacKey. 1999. Common resistance mechanisms to deoxynucleoside analogues in variants of the human erythroleukaemic line K562. *Br J Haematol* 106:78-85.
43. Lee, J. J., C. H. Maeng, S. K. Baek, G. Y. Kim, J. H. Yoo, C. W. Choi, Y. H. Kim, Y. T. Kwak, D. H. Kim, Y. K. Lee, J. B. Kim, and S. Y. Kim. The

immunohistochemical overexpression of ribonucleotide reductase regulatory subunit M1 (RRM1) protein is a predictor of shorter survival to gemcitabine-based chemotherapy in advanced non-small cell lung cancer (NSCLC). *Lung Cancer* 70:205-210.

44. Kim, S. O., J. Y. Jeong, M. R. Kim, H. J. Cho, J. Y. Ju, Y. S. Kwon, I. J. Oh, K. S. Kim, Y. I. Kim, S. C. Lim, and Y. C. Kim. 2008. Efficacy of gemcitabine in patients with non-small cell lung cancer according to promoter polymorphisms of the ribonucleotide reductase M1 gene. *Clin Cancer Res* 14:3083-3088.
45. Davidson, J. D., L. Ma, M. Flagella, S. Geeganage, L. M. Gelbert, and C. A. Slapak. 2004. An increase in the expression of ribonucleotide reductase large subunit 1 is associated with gemcitabine resistance in non-small cell lung cancer cell lines. *Cancer Res* 64:3761-3766.
46. Rosell, R., K. D. Danenberg, V. Alberola, G. Bepler, J. J. Sanchez, C. Camps, M. Provencio, D. Isla, M. Taron, P. Diz, and A. Artal. 2004. Ribonucleotide reductase messenger RNA expression and survival in gemcitabine/cisplatin-treated advanced non-small cell lung cancer patients. *Clin Cancer Res* 10:1318-1325.
47. Duxbury, M. S., H. Ito, M. J. Zinner, S. W. Ashley, and E. E. Whang. 2004. RNA interference targeting the M2 subunit of ribonucleotide reductase enhances pancreatic adenocarcinoma chemosensitivity to gemcitabine. *Oncogene* 23:1539-1548.

48. Ng, S. S. W., M. S. Tsao, S. Chow, and D. W. Hedley. 2000. Inhibition of phosphatidylinositide 3-kinase enhances gemcitabine-induced apoptosis in human pancreatic cancer cells. *Cancer Res* 60:5451-5455.
49. Ng, S. S., M. S. Tsao, T. Nicklee, and D. W. Hedley. 2001. Wortmannin inhibits pkb/akt phosphorylation and promotes gemcitabine antitumor activity in orthotopic human pancreatic cancer xenografts in immunodeficient mice. *Clin Cancer Res* 7:3269-3275.
50. Duxbury, M. S., H. Ito, M. J. Zinner, S. W. Ashley, and E. E. Whang. 2004. Focal adhesion kinase gene silencing promotes anoikis and suppresses metastasis of human pancreatic adenocarcinoma cells. *Surgery* 135:555-562.
51. Duxbury, M. S., H. Ito, M. J. Zinner, S. W. Ashley, and E. E. Whang. 2004. siRNA directed against c-Src enhances pancreatic adenocarcinoma cell gemcitabine chemosensitivity. *J Am Coll Surg* 198:953-959.
52. Duxbury, M. S., H. Ito, M. J. Zinner, S. W. Ashley, and E. E. Whang. 2004. Inhibition of SRC tyrosine kinase impairs inherent and acquired gemcitabine resistance in human pancreatic adenocarcinoma cells. *Clin Cancer Res* 10:2307-2318.
53. Shah, A. N., and G. E. Gallick. 2007. Src, chemoresistance and epithelial to mesenchymal transition: are they related? *Anticancer Drugs* 18:371-375.
54. Mahon, P. C., P. Baril, V. Bhakta, C. Chelala, K. Caulee, T. Harada, and N. R. Lemoine. 2007. S100A4 contributes to the suppression of BNIP3

- expression, chemoresistance, and inhibition of apoptosis in pancreatic cancer. *Cancer Res* 67:6786-6795.
55. Erkan, M., J. Kleeff, I. Esposito, T. Giese, K. Ketterer, M. W. Buchler, N. A. Giese, and H. Friess. 2005. Loss of BNIP3 expression is a late event in pancreatic cancer contributing to chemoresistance and worsened prognosis. *Oncogene* 24:4421-4432.
 56. Cascallo, M., J. Calbo, G. Capella, C. Fillat, M. Pastor-Anglada, and A. Mazo. 2005. Enhancement of gemcitabine-induced apoptosis by restoration of p53 function in human pancreatic tumors. *Oncology* 68:179-189.
 57. Galmarini, C. M., M. L. Clarke, N. Falette, A. Puisieux, J. R. Mackey, and C. Dumontet. 2002. Expression of a non-functional p53 affects the sensitivity of cancer cells to gemcitabine. *Int J Cancer* 97:439-445.
 58. Kielb, S. J., N. L. Shah, M. A. Rubin, and M. G. Sanda. 2001. Functional p53 mutation as a molecular determinant of paclitaxel and gemcitabine susceptibility in human bladder cancer. *J Urol* 166:482-487.
 59. Huang, P., S. Chubb, L. W. Hertel, G. B. Grindey, and W. Plunkett. 1991. Action of 2',2'-difluorodeoxycytidine on DNA synthesis. *Cancer Res* 51:6110-6117.
 60. Gandhi, V., J. Legha, F. Chen, L. W. Hertel, and W. Plunkett. 1996. Excision of 2',2'-difluorodeoxycytidine (gemcitabine) monophosphate residues from DNA. *Cancer Res* 56:4453-4459.

61. Lin, X., and S. B. Howell. 1999. Effect of loss of DNA mismatch repair on development of topotecan-, gemcitabine-, and paclitaxel-resistant variants after exposure to cisplatin. *Mol Pharmacol* 56:390-395.
62. Ewald, B., D. Sampath, and W. Plunkett. 2008. ATM and the Mre11-Rad50-Nbs1 complex respond to nucleoside analogue-induced stalled replication forks and contribute to drug resistance. *Cancer Res* 68:7947-7955.
63. Rothstein, R., B. Michel, and S. Gangloff. 2000. Replication fork pausing and recombination or "gimme a break". *Genes Dev* 14:1-10.
64. Petermann, E., M. L. Orta, N. Issaeva, N. Schultz, and T. Helleday. Hydroxyurea-stalled replication forks become progressively inactivated and require two different RAD51-mediated pathways for restart and repair. *Mol Cell* 37:492-502.
65. Helleday, T. 2003. Pathways for mitotic homologous recombination in mammalian cells. *Mutat Res* 532:103-115.
66. Bryant, H. E., E. Petermann, N. Schultz, A. S. Jemth, O. Loseva, N. Issaeva, F. Johansson, S. Fernandez, P. McGlynn, and T. Helleday. 2009. PARP is activated at stalled forks to mediate Mre11-dependent replication restart and recombination. *Embo Journal* 28:2601-2615.
67. Saintigny, Y., F. Delacote, G. Vares, F. Petitot, S. Lambert, D. Averbek, and B. S. Lopez. 2001. Characterization of homologous recombination induced by replication inhibition in mammalian cells. *EMBO J* 20:3861-3870.
68. Negrini, S., V. G. Gorgoulis, and T. D. Halazonetis. Genomic instability--an evolving hallmark of cancer. *Nat Rev Mol Cell Biol* 11:220-228.

69. Arias-Lopez, C., I. Lazaro-Trueba, P. Kerr, C. J. Lord, T. Dexter, M. Iravani, A. Ashworth, and A. Silva. 2006. p53 modulates homologous recombination by transcriptional regulation of the RAD51 gene. *EMBO Rep* 7:219-224.
70. Friedler, A., D. B. Veprintsev, T. Rutherford, K. I. von Glos, and A. R. Fersht. 2005. Binding of Rad51 and other peptide sequences to a promiscuous, highly electrostatic binding site in p53. *J Biol Chem* 280:8051-8059.
71. Buchhop, S., M. K. Gibson, X. W. Wang, P. Wagner, H. W. Sturzbecher, and C. C. Harris. 1997. Interaction of p53 with the human Rad51 protein. *Nucleic Acids Res* 25:3868-3874.
72. Lim, D. S., and P. Hasty. 1996. A mutation in mouse rad51 results in an early embryonic lethal that is suppressed by a mutation in p53. *Mol Cell Biol* 16:7133-7143.
73. Sturzbecher, H. W., B. Donzelmann, W. Henning, U. Knippschild, and S. Buchhop. 1996. p53 is linked directly to homologous recombination processes via RAD51/RecA protein interaction. *EMBO J* 15:1992-2002.
74. Field, S. B., and N. M. Bleehen. 1979. Hyperthermia in the Treatment of Cancer. *Cancer Treatment Reviews* 6:63-94.
75. Palzer, R. J., and C. Heidelberger. 1973. Influence of drugs and synchrony on the hyperthermic killing of HeLa cells. *Cancer Res* 33:422-427.
76. Zaalishvili, G., E. Zaldastanishvili, M. Karapetian, and T. Zaalishvili. Increased PARP-1 levels in nuclear matrix isolated from heat shock treated rat liver. *Biochemistry (Mosc)* 77:105-110.

77. Martin, N., K. Schwamborn, V. Schreiber, A. Werner, C. Guillier, X. D. Zhang, O. Bischof, J. S. Seeler, and A. Dejean. 2009. PARP-1 transcriptional activity is regulated by sumoylation upon heat shock. *EMBO J* 28:3534-3548.
78. Zhu, W. G., J. D. Seno, B. D. Beck, and J. R. Dynlacht. 2001. Translocation of MRE11 from the nucleus to the cytoplasm as a mechanism of radiosensitization by heat. *Radiat Res* 156:95-102.
79. Seno, J. D., and J. R. Dynlacht. 2004. Intracellular redistribution and modification of proteins of the Mre11/Rad50/Nbs1 DNA repair complex following irradiation and heat-shock. *J Cell Physiol* 199:157-170.
80. Gerashchenko, B. I., G. Gooding, and J. R. Dynlacht. Hyperthermia alters the interaction of proteins of the Mre11 complex in irradiated cells. *Cytometry A* 77:940-952.
81. Dynlacht, J. R., C. N. Batuello, J. T. Lopez, K. K. Kim, and J. J. Turchi. Identification of Mre11 as a target for heat radiosensitization. *Radiat Res* 176:323-332.
82. Schlacher, K., N. Christ, N. Siaud, A. Egashira, H. Wu, and M. Jasin. Double-strand break repair-independent role for BRCA2 in blocking stalled replication fork degradation by MRE11. *Cell* 145:529-542.
83. Krawczyk, P. M., B. Eppink, J. Essers, J. Stap, H. Rodermond, H. Odijk, A. Zelensky, C. van Bree, L. J. Stalpers, M. R. Buist, T. Soullie, J. Rens, H. J. Verhagen, M. J. O'Connor, N. A. Franken, T. L. Ten Hagen, R. Kanaar, and J. A. Aten. Mild hyperthermia inhibits homologous recombination, induces

- BRCA2 degradation, and sensitizes cancer cells to poly (ADP-ribose) polymerase-1 inhibition. *Proc Natl Acad Sci U S A* 108:9851-9856.
84. Xian Ma, Y., S. Fan, J. Xiong, R. Q. Yuan, Q. Meng, M. Gao, I. D. Goldberg, S. A. Fuqua, R. G. Pestell, and E. M. Rosen. 2003. Role of BRCA1 in heat shock response. *Oncogene* 22:10-27.
85. Franken, N. A., H. M. Rodermond, J. Stap, J. Haveman, and C. van Bree. 2006. Clonogenic assay of cells in vitro. *Nat Protoc* 1:2315-2319.
86. Glazer, E. S., C. Zhu, K. L. Massey, C. S. Thompson, W. D. Kaluarachchi, A. N. Hamir, and S. A. Curley. Noninvasive radiofrequency field destruction of pancreatic adenocarcinoma xenografts treated with targeted gold nanoparticles. *Clin Cancer Res* 16:5712-5721.
87. Warters, R. L., and O. L. Stone. 1983. The effects of hyperthermia on DNA replication in HeLa cells. *Radiat Res* 93:71-84.
88. Mane, J. M., A. Sancho, A. Munoz, I. Rubio, R. Fernandez, S. Carrera, N. Fuente, D. Ballesteros, R. Casas, I. Marrodan, X. Mielgo, and G. Lopez-Vivanco. Fixed-dose-rate gemcitabine infusion in patients with advanced pancreatic or biliary tree adenocarcinoma. *Tumori* 96:405-410.
89. Vertrees, R. A., G. C. Das, V. L. Popov, A. M. Coscio, T. J. Goodwin, R. Logrono, J. B. Zwischenberger, and P. J. Boor. 2005. Synergistic interaction of hyperthermia and Gemcitabine in lung cancer. *Cancer Biol Ther* 4:1144-1153.
90. Van Bree, C., C. Beumer, H. M. Rodermond, J. Haveman, and P. J. Bakker. 1999. Effectiveness of 2',2'difluorodeoxycytidine (Gemcitabine) combined

- with hyperthermia in rat R-1 rhabdomyosarcoma in vitro and in vivo. *Int J Hyperthermia* 15:549-556.
91. Hirooka, Y., S. Shiota, T. Matsui, Y. Murata, H. Hiraoka, A. Kimura, Y. Iitsuka, and S. Koga. 1990. The effects of hyperthermia on the cell cycle of Ehrlich ascites cancer cells in vivo. *Jpn J Surg* 20:437-442.
 92. Bhuyan, B. K., K. J. Day, C. E. Edgerton, and O. Ogunbase. 1977. Sensitivity of different cell lines and of different phases in the cell cycle to hyperthermia. *Cancer Res* 37:3780-3784.
 93. Ying, S., F. C. Hamdy, and T. Helleday. Mre11-dependent degradation of stalled DNA replication forks is prevented by BRCA2 and PARP1. *Cancer Res.*
 94. Su, X., J. A. Bernal, and A. R. Venkitaraman. 2008. Cell-cycle coordination between DNA replication and recombination revealed by a vertebrate N-end rule degron-Rad51. *Nat Struct Mol Biol* 15:1049-1058.
 95. Jensen, R. B., A. Carreira, and S. C. Kowalczykowski. Purified human BRCA2 stimulates RAD51-mediated recombination. *Nature* 467:678-683.

Vita

Mustafa Raoof was born in Tabuk, Saudi Arabia. After completing his schooling at Adamjee Government Science College, Pakistan in 2001, he entered Aga Khan University Medical College. He received his medical degree (M.B, B.S) with honors in 2006. During the following year, he pursued basic science research at Beth Israel Deaconess Medical Center, Harvard Medical School working on several projects in trauma immunology. During 2008-2009, he completed his general surgery internship at Yale University and entered general surgery residency at University of Arizona in July 2009. In July 2010, he took a two-year sabbatical to pursue a postdoctoral research fellowship at M.D. Anderson Cancer Center. During the same time, in January 2011, he entered the Graduate School of Biomedical Sciences at The University of Texas Health Science Center, Houston.

Permanent Address:

166/1 Khayaban-e-Shaheen

Karachi, Pakistan 775500